Solvent and Secondary Kinetic Isotope Effects for the Microhydrated SN2 Reaction of Cl-(H2O)N with CH3Cl

ARTICLE *in* JOURNAL OF THE AMERICAN CHEMICAL SOCIETY · JANUARY 1991

Impact Factor: 12.11 · DOI: 10.1021/ja00003a015

3 AUTHORS, INCLUDING:

Donald Truhlar
University of Minnesota Twin Cities
1,342 PUBLICATIONS **79,615** CITATIONS

photoelectron data suggest that the weakly bound butadiene state does not interact significantly with the molybdenum surface since it has a rather high C(1s) binding energy (~285 eV). Butadiene directly bound to the surface is expected to have a lower C(1s) binding energy due to final state screening. Interestingly, ethylene sulfide deposits 0.32 monolayer of sulfur during reaction, compared to 0.23 for 2,5-DHT and ~0.1 for tetrahydrothiophene and thiophene. Consistent with this explanation, in the case of ethylene sulfide, ethylene is directly evolved into the gas phase at 100 K so that the product does not occupy surface sites. In contrast, both tetrahydrothiophene and thiophene initially form strongly bound products.

The marked dependence of the reaction selectivity on the initial exposure of 2,5-dihydrothiophene (Figure 3) may be caused by a modification of the surface activity as the coverage of reaction products, such as sulfur and/or hydrocarbon fragments, increases. In experiments explicitly examining the effects of surface sulfur on desulfurization reactions, the presence of adsorbed sulfur was found to slow the kinetics for nonselective reaction of both sulfur-containing and hydrocarbon reaction intermediates on Mo(110).[32] A similar effect is proposed here since we have shown experimentally that some nonselective reaction occurs upon adsorption at 120 K. Since this process is apparently not reversible, postulated changes in adsorbate structure induced by intermolecular interactions at high coverage, thought to be important in the reactions of large thiols on Mo(110),[19] are not necessary for explaining coverage-dependent selectivities in the case of 2,5-dihydrothiophene.

The presence of *molecular* 2,5-dihydrothiophene on the surface also appears to modify the kinetics for butadiene elimination. A pronounced maximum in the rate of butadiene evolution is observed just above the 2,5-DHT desorption peak near 210 K for large initial 2,5-DHT exposures (relative exposure > 0.8) (Figure 1). The coincidence of a maximum in the rate of butadiene elimination with the trailing edge of 2,5-DHT desorption suggests that 2,5-dihydrothiophene modifies its own reaction kinetics either through effects on the local electronic structure or by site blocking.

Conclusions. 2,5-Dihydrothiophene readily eliminates butadiene during temperature-programmed reaction on Mo(110). Approximately two-thirds of the irreversibly adsorbed 2,5-DHT yields gaseous butadiene and adsorbed sulfur via an intramolecular elimination process, while one-third is nonselectively decomposed on the surface without producing any gas-phase hydrocarbons. Selective desulfurization to form gaseous butadiene is favored at high initial 2,5-DHT coverages, possibly because of a moderation of the surface activity as decomposition products, such as sulfur, are deposited during reaction. The differences between the reactivity of 2,5-DHT and those of thiophene and tetrahydrothiophene are attributed largely to the fact that intramolecular elimination is kinetically more favorable for 2,5-DHT. Only minimal reorganization is required along the path for butadiene formation from 2,5-DHT, while thiophene has no stable gaseous elimination product and cyclobutane formation from tetrahydrothiophene would require substantial displacement of the carbons bound to the sulfur. These findings are generally consistent with previous studies of 2,5-DHT reactivity on high surface area catalysts and in organometallic complexes.

Acknowledgment. The 2,5-dihydrothiophene used in these experiments was kindly provided by Prof. R. J. Angelici of Iowa State University and was synthesized by Moon-Gun Choi. Funding for this research was provided by the Department of Energy, Basic Energy Sciences, Grant DE-FG02-84ER13289.

(32) Wiegand, B. C.; Roberts, J. T.; Friend, C. M. Unpublished results.

Solvent and Secondary Kinetic Isotope Effects for the Microhydrated S_N2 Reaction of $Cl^-(H_2O)_n$ with CH_3Cl

Xin Gui Zhao, Susan C. Tucker,† and Donald G. Truhlar*

Contribution from the Department of Chemistry, Chemical Physics Program, and Supercomputer Institute, University of Minnesota, Minneapolis, Minnesota 55455-0431. *Received May 21, 1990. Revised Manuscript Received September 27, 1990*

Abstract: We have calculated gas-phase rate coefficients and deuterium kinetic isotope effects (KIEs) for isotopic substitution in either the methyl group or the water of the title reaction with $n = 1$ and 2. The calculations are carried out by variational transition-state theory with semiclassical transmission coefficients, and they are based on 27- and 36-dimensional reaction-path potentials presented previously. A critical aspect of the potentials is that the solute part is based on high-level ab initio calculations. We also analyze the effect of deuterium substitution at methyl for the case of $n = 0$. We calculate an inverse effect for substitution at methyl both for bare solute ($n = 0$) and for microhydrated solute with $n = 1$ or 2. A detailed mode analysis shows that the inverse effect for the unhydrated reaction is dominated by C–H stretch contributions rather than by CH_3 deformations as is usually assumed in analyzing experimental data on solution-phase reactions. Furthermore, the C–H stretch contribution to the inverse α-deuterium KIE is essentially unaffected by microhydration. We find that for $n = 1$ the secondary KIE for substitution at methyl is larger than the solvent KIE, but for $n = 2$ the trend is reversed. The solvent KIEs are also interpreted in terms of the contributions of individual vibrational modes; in the $n = 2$ case the KIE is attributable to the breaking of a water–water hydrogen bond and the weakening of a water–chloride hydrogen bond.

Introduction

Gas-phase reactions of microhydrated ions provide opportunities for exploring fundamental concepts of condensed-phase kinetics using the techniques, both experimental and theoretical, of few-body gas-phase dynamics.[1-12] In previous work[12] we have cal-

* Author to whom correspondence should be addressed.
† Current address: Department of Chemistry, Columbia University, New York, NY 10027.

(1) Fehsenfeld, F. C.; Ferguson, E. E. *J. Chem. Phys.* **1974**, *61*, 3181. Fehsenfeld, F. C.; Dotan, I.; Albritton, D. L.; Howard, C. J.; Ferguson, E. E. *J. Geophys. Res.* **1978**, *33*, 1333. Bohringer, H.; Fahey, D. W.; Fehsenfeld, F. C.; Ferguson, E. E. *Planet Space Sci.* **1983**, *31*, 185.

0002-7863/91/1513-826$02.50/0

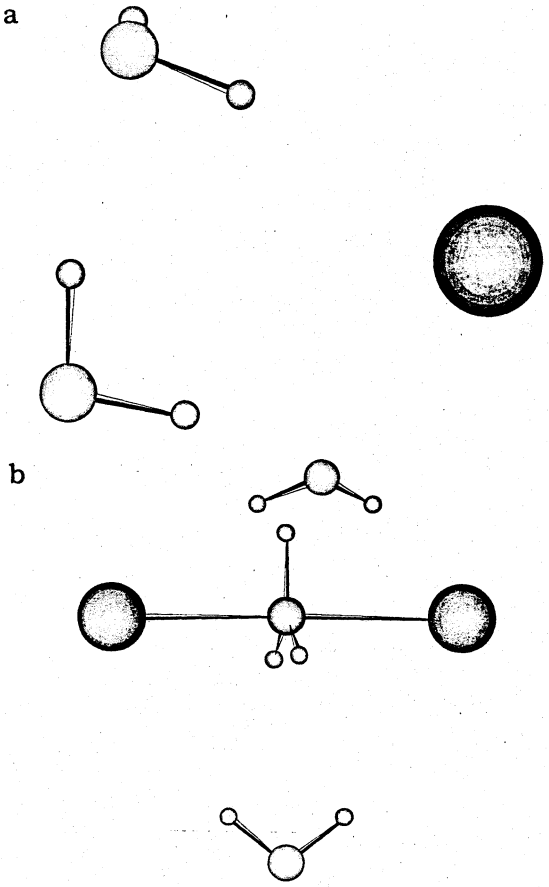

Figure 1. (a) Structure of $Cl^-(H_2O)_2$. (b) Structure of $Cl{-}CH_3{-}Cl^-(H_2O)_2$ at the saddle point.

culated the variational transition-state-theory rate constant for the reactions

$$Cl^-(H_2O)_n + CH_3Cl' \rightarrow ClCH_3 + Cl'^-(H_2O)_n \quad (R1)$$

with $n = 0$, 1, and 2 and for

$$Cl^-(H_2O)_n + CD_3Cl' \rightarrow ClCD_3 + Cl'^-(H_2O)_n \quad (R2)$$

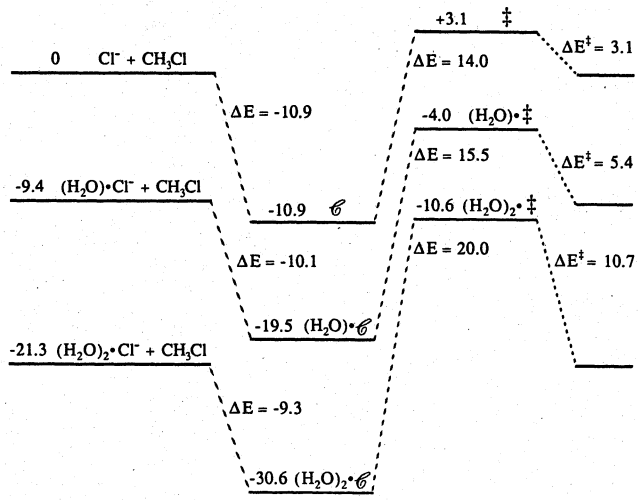

Figure 2. Reaction energetics, in kcal/mol on an energy scale having the zero of energy at infinitely separated $H_2O + H_2O + Cl^- + CH_3Cl$, for reaction R2 with $n = 0$, 1, and 2. For all reactions the ion–dipole complex on the product side has been omitted from the diagram since its energy is identical with that of the reactant-side complex.

with $n = 0$. A major focus of that work was to test the hypothesis of "equilibrium solvation". In the present paper we focus on kinetic isotope effects (KIEs) for such microsolvated reactions, and we extend the previous calculations to include reaction R2 with $n = 1$ and 2 and the reaction

$$Cl^-(D_2O)_n + CH_3Cl' \rightarrow ClCH_3 + Cl'^-(D_2O)_n \quad (R3)$$

also with $n = 1$ and 2. These calculations are used to gain insight about the coupling of solutes to first-hydration-shell molecules in charge migration reactions. In addition, since such gas-phase cluster ion reactions are of great experimental[1-7] interest, we hope that our predictions will be tested experimentally.

Methods

The dynamical calculations involve three steps: (i) choice of potential energy function, (ii) variational transition-state-theory calculations with quantized vibrations and classical rotational and reaction-coordinate motions, and (iii) inclusion of tunneling effects by a multidimensional semiclassical ground-state transmission coefficient.

(i) The potential energy function for the present study is taken from previous work[12] by two of the authors. In particular, for $n = 0$, it is a semiglobal analytic representation of ab initio electronic structure calculations at the MP2/6-31G(d,p) level[13,14] with empirical adjustment of the saddle point height to the experimental rate constant of Barlow et al.[15] For $n > 0$ the water and water–dimer potential are based[12] on the work of Watts and co-workers,[16] and the water–solute interactions are included[12] by using atom–atom potential parameters developed by Clementi and co-workers,[17] plus charge–charge interactions. All degrees of freedom are treated as nonrigid, giving 18, 27, and 36 degrees of freedom for $n = 0$, 1, and 2, respectively.

The resulting potential function for $n = 0$ has a classical binding energy of 11.0 kcal/mol for the ion–dipole complex and a 3.1 kcal/mol symmetric barrier with respect to reactants (14.1 kcal/mol with respect to the precursor and successor complexes.) Adding one or two water molecules increases the barrier with respect to reactants to 5.4 and 10.7 kcal/mol, respectively. The first water of hydration forms a hydrogen bond to Cl^- in reactants and bridges the CH_3 group (between two C–H bonds) to form partial hydrogen bonds to both partially charged chlorides at the transition state. The solvation structure of the reactant and the

(2) Bohme, D. K.; Mackay, G. I.; Tanner, S. D. *J. Am. Chem. Soc.* **1979**, *101*, 3724. Tanner, S. D.; Mackay, G. I.; Bohme, D. K. *Can. J. Chem.* **1981**, *59*, 1615. Bohme, D. K.; Mackay, G. I. *J. Am. Chem. Soc.* **1981**, *103*, 978. Bohme, D. K.; Rakshit, A. B.; Mackay, G. I. *J. Am. Chem. Soc.* **1982**, *104*, 1100. Bohme, D. K.; Raksit, A. B. *J. Am. Chem. Soc.* **1984**, *106*, 3447; *Can. J. Chem.* **1985**, *63*, 3007.

(3) Smith, D.; Adams, N. G.; Henchman, M. J. *J. Chem. Phys.* **1980**, *72*, 4951. Henchman, M.; Paulson, J. F.; Hierl, P. M. *J. Am. Chem. Soc.* **1983**, *105*, 5509. Henchman, M.; Hierl, P. M.; Paulson, J. F. *J. Am. Chem. Soc.* **1985**, *107*, 2812. Hierl, P. M.; Ahrens, A. F.; Henchman, M.; Viggiano, A. A.; Paulson, J. F. *J. Am. Chem. Soc.* **1986**, *108*, 3140, 3142. Henchman, M.; Hierl, P. M.; Paulson, J. F. *ACS Adv. Chem. Ser.* **1987**, *215*, 83. Hierl, P. M.; Ahrens, A. F.; Henchman, M. J.; Viggiano, A. A.; Paulson, J. F.; Clary, D. C. *Faraday Discuss. Chem. Soc.* **1988**, *85*, 37.

(4) Caldwell, G.; Rozeboom, M. D.; Kiplinger, J. P.; Bartmess, J. E. *J. Am. Chem. Soc.* **1984**, *106*, 809.

(5) Lane, K. R.; Squires, R. R. *J. Am. Chem. Soc.* **1986**, *108*, 7187.

(6) Kebarle, P.; Dillow, G. W.; Hirao, K.; Chowdhury, S. *Faraday Discuss. Chem. Soc.* **1988**, *85*, 23.

(7) Baer, S.; Stoutland, P. O.; Brauman, J. I. *J. Am. Chem. Soc.* **1989**, *111*, 4097.

(8) Cremaschi, P.; Gamba, A.; Simonetta, M. *Theor. Chim. Acta* **1972**, *25*, 237.

(9) Morokuma, K. *J. Am. Chem. Soc.* **1982**, *104*, 3732. Ohta, K.; Morokuma, K. *J. Phys. Chem.* **1985**, *89*, 5845.

(10) Jaume, J.; Lluch, J. M.; Oliva, A.; Bertrán, J. *Chem. Phys. Lett.* **1984**, *106*, 232. Bertrán, J. In *New Theoretical Concepts for Understanding Organic Reactivity*; Bertrán, J., Csizmadia, I. G., Eds.; Kluwer: Dordrecht, 1989; p 291.

(11) Kong, Y. S.; Jhon, M. S. *Theor. Chim. Acta* **1986**, *70*, 123.

(12) Tucker, S. C.; Truhlar, D. G. *J. Am. Chem. Soc.* **1990**, *112*, 3338, 3347. Note that in this reference the KIE is discussed in terms of k_D/k_H whereas here we use the more standard k_H/k_D convention throughout.

(13) Hehre, W. J.; Radom, L.; Schleyer, P. v. R.; Pople, J. A. *Ab Initio Molecular Orbital Theory*; Wiley: New York, 1986.

(14) Tucker, S. C.; Truhlar, D. G. *J. Phys. Chem.* **1989**, *93*, 8138.

(15) Barlow, S. E.; Van Doren, J. M.; Bierbaum, V. M. *J. Am. Chem. Soc.* **1988**, *110*, 7240.

(16) Reimers, J. R.; Watts, R. O.; Klein, M. L. *Chem. Phys.* **1982**, *64*, 95. Reimers, J. R.; Watts, R. O. *Mol. Phys.* **1984**, *52*, 357. Coker, D. F.; Miller, R. E.; Watts, R. O. *J. Chem. Phys.* **1985**, *82*, 3554.

(17) Kistenmacher, H.; Popkie, H.; Clementi, E. *J. Chem. Phys.* **1973**, *59*, 5842. Clementi, E.; Cavallone, F.; Scordamaglia, R. *J. Am. Chem. Soc.* **1977**, *99*, 5531.

Table I. Rate Constants (cm^3 $molecule^{-1}$ s^{-1}) and Kinetic Isotope Effects at 300 K As Calculated by Conventional Transition-State Theory (‡), Improved Canonical Variational Theory (CVT), and Canonical Variational Theory Corrected for Tunneling (CVT/SCSAG)

	‡		CVT		CVT/SCSAG	
reaction	k	k_H/k_D	k	k_H/k_D	k	k_H/k_D
1. $Cl^- + CH_3Cl$	2.36×10^{-14}		2.28×10^{-14}		3.58×10^{-14}	
2. $Cl^- + CD_3Cl$	2.46×10^{-14}	0.96	2.38×10^{-14}	0.96	3.78×10^{-14}	0.95
3. $Cl^-(H_2O) + CH_3Cl$	6.38×10^{-18}		6.27×10^{-18}		1.09×10^{-17}	
4. $Cl^-(H_2O) + CD_3Cl$	6.73×10^{-18}	0.95	6.62×20^{-18}	0.95	1.15×10^{-17}	0.94
5. $Cl^-(D_2O) + CH_3Cl$	6.15×10^{-18}	1.04	6.04×10^{-18}	1.04	1.05×10^{-17}	1.04
6. $Cl^-(H_2O)_2 + CH_3Cl$	2.07×10^{-20}		2.05×10^{-20}		3.70×20^{-20}	
7. $Cl^-(H_2O)_2 + CD_3Cl$	2.23×10^{-20}	0.93	2.21×10^{-20}	0.93	4.05×10^{-20}	0.91
8. $Cl^-(D_2O)_2 + CH_3Cl$	1.65×10^{-20}	1.26	1.63×10^{-20}	1.26	2.99×10^{-20}	1.24

saddle point for $n = 2$ are shown in Figure 1; the structures for $n = 1$ are similar but with one water missing. Notice the presence of a water–water hydrogen bond in $Cl^-(H_2O)_2$ but not in the transition state.

(ii) Variational transition-state-theory[18-22] (VTST) calculations are carried out by canonical variational theory[19-21] (CVT) with quantized harmonic vibrations. (Improved canonical variational transition-state-theory[20,21] calculations were also carried out in all cases, and they gave essentially the same results. Thus we present only the simpler CVT calculations.) CVT involves first calculating the isotope-dependent minimum energy reaction path and the free energy of activation profile[20] as a function the displacement s along the reaction path and then locating the variational transition state at the maximum of this profile. For comparison with the CVT rate constant, denoted $k^{CVT}(T)$, we also calculated the rate constant by conventional transition-state theory,[21-23] and this result is denoted $k^{\ddagger}(T)$. We use the POLYRATE program,[24] developed in our laboratory, for both sets of calculations. We do *not* assume equilibrium solvation but rather we treat all degrees of freedom of both solute and solvent in the same footing without this additional assumption.

(iii) The final VTST rate constant is given by

$$k^{CVT/SCSAG}(T) = \kappa^{SC}(T)k^{CVT}(T) \quad (1)$$

where $\kappa^{SC}(T)$ is a transmission coefficient[20,21] calculated by the Small–Curvature Semiclassical Adiabatic Ground-State[21,25] method. This transmission coefficient corrects the theory for quantal effects on the reaction-coordinate motion, especially tunneling.

All calculations were converged with respect to numerical parameters to the full number of significant figures shown in the tables, and kinetic isotope effects were calculated from unrounded results. After the saddle point was located by the Newton–Raphson method, the reaction path along the minimum-energy path (MEP) was computed by following the negative of the gradient of the potential, in a mass-scaled coordinate system[20] with $\mu = 1$ amu, from the saddle point to the reactant and from the saddle point to the product. In all of our calculations, the negative gradient was followed using an Euler single-step integrator with a step size δs of 5×10^{-5} a_0 for the first 2000 steps in each direction and then a step size of 10^{-3} a_0. At intervals of 5×10^{-3} a_0 (reactions 1 and 2) or 10^{-2} a_0 (reactions 3–8) along the reaction paths, the hessian matrix of quadratic force constants was computed to obtain the generalized normal mode frequencies, the reaction path curvature, and the ground-state vibrationally adiabatic potential. Then, at the same intervals, the free energy of activation profile was evaluated and interpolated to get the generalized transition-state rate constants. The tunneling correction was evaluated using repeated Kronrod quadrature for both the $\theta(E)$ integral over s (eq 94 of ref 21) and the Boltzmann average (eq 91 of ref 21). The ranges of the integrals were divided into two equal segments and 61-point (reactions 1 and 2) or 81-point (reactions 3–8) Kronrod quadrature was used in each segment for both the $\theta(E)$ integral and the Boltzmann integral. The calculations were carried out on the Cray X-MP/4-16 computer at the Minnesota Supercomputer Institute.

Table II. Kinetic Isotope Effects k_H/k_D as Functions of Temperature (CVT/SCSAG)

		T (K)				
reaction	KIE	200	300	400	600	1000
2. $Cl^- + CD_3Cl$	k_1/k_2	0.91	0.95	0.95	0.94	0.96
4. $Cl^-(H_2O) + CD_3Cl$	k_3/k_4	0.90	0.94	0.95	0.95	0.96
5. $Cl^-(D_2O) + CH_3Cl$	k_3/k_5	1.04	1.04	1.03	1.02	1.01
7. $Cl^-(H_2O)_2 + CD_3Cl$	k_6/k_7	0.85	0.91	0.93	0.94	0.95
8. $Cl^-(D_2O)_2 + CH_3Cl$	k_6/k_8	1.55	1.24	1.12	1.03	0.99

Table III. Arrhenius Preexponential Factor A (cm^3 $molecule^{-1}$ s^{-1}) and Activation Energy (kcal/mol) at 300 K[a] from CVT/SCSAG Calculations

reaction	A	E_a
1. $Cl^- + CH_3Cl$	5.21×10^{-12}	2.97
2. $Cl^- + CD_3Cl$	5.33×10^{-12}	2.95
3. $Cl^-(H_2O) + CH_3Cl$	2.56×10^{-13}	6.00
4. $Cl^-(H_2O) + CD_3Cl$	2.58×10^{-13}	5.97
5. $Cl^-(D_2O) + CH_3Cl$	2.53×10^{-13}	6.01
6. $Cl^-(H_2O)_2 + CH_3Cl$	2.48×10^{-12}	10.7
7. $Cl^-(H_2O)_2 + CD_3Cl$	2.46×10^{-12}	10.7
8. $Cl^-(D_2O)_2 + CH_3Cl$	3.12×10^{-12}	11.0

[a] Computed by fitting to $k = A \exp(-E_a/RT)$ at 295 and 305 K.

Results

The conventional and variational transition-state-theory rate constants and kinetic isotope effects (k_H/k_D) at 300 K are given in Table I. Since the effect of hydration on the unsubstituted (i.e., perprotio) reactions has been discussed previously,[12] we concentrate our attention on the effect of isotopic substitution. First of all we see that the deviation of variational from conventional transition-state theory and the extent of tunneling are approximately independent of isotopic substitution so we can use any of the three levels of theory; we will use the most reliable level, CVT/SCSAG.

Reactions 2, 4, and 7 show the effect of α-deuterium substitution at the reaction center. The isotope effect is inverse ($k_H/k_D < 1$). Interestingly, the deviation of k_H/k_D from unity is almost twice as large with two waters present ($n = 2$) as for the bare solute ($n = 0$); this trend as well as the reason for the inverse effect will be analyzed below.

Reactions 5 and 8 show the effect of using heavy water. The KIE is particularly large for $n = 2$.

Table II shows that most of the KIEs are only weakly dependent on temperature, with the heavy-water effect for $n = 2$ providing a striking exception. Table III presents Arrhenius activation parameters for all reactions, and it shows that addition of a second heavy water has significant effect on both Arrhenius parameters.

(18) Wigner, E. *J. Chem. Phys.* **1937**, *5*, 720. Keck, J. C. *Adv. Chem. Phys.* **1967**, *13*, 85. Truhlar, D. G.; Garrett, B. C. *Acc. Chem. Res.* **1980**, *13*, 440.

(19) Garrett, B. C.; Truhlar, D. G. *J. Chem. Phys.* **1979**, *70*, 1593; *J. Phys. Chem.* **1979**, *83*, 1079.

(20) Garrett, B. C.; Truhlar, D. G.; Grev, R. S.; Magnuson, A. W. *J. Phys. Chem.* **1980**, *84*, 1730.

(21) Truhlar, D. G.; Isaacson, A. D.; Garrett, B. C. In *Theory of Chemical Reaction Dynamics*; Baer, M., Ed.; CRC Press: Boca Raton, FL, 1985; Vol. IV, p 65.

(22) Kreevoy, M. M.; Truhlar, D. G. In *Investigation of Rates and Mechanisms of Reactions*, 4th ed., Part I; Bernasconi, C. F., Ed.; Wiley: New York, 1986; p 13. Tucker, S. C.; Truhlar, D. G. In *New Theoretical Concepts for Understanding Organic Reactions*; Bertrán, J., Csizmadia, I. G., Eds.; Kluwer: Dordrecht, 1989; p 291.

(23) Eyring, H. *J. Chem. Phys.* **1935**, *3*, 107.

(24) Isaacson, A. D.; Truhlar, D. G.; Rai, S. N.; Steckler, R.; Hancock, G. C.; Garrett, B. C.; Redmon, M. *J. Comput. Phys. Commun.* **1987**, *47*, 91. Isaacson, A. D.; Truhlar, D. G.; Rai, S. N.; Hancock, G. C.; Lauderdale, J. G.; Truong, T. N.; Joseph, T.; Garrett, B. C.; Steckler, R. *Research Report UMSI 88/87*, University of Minnesota Supercomputer Institute, Minneapolis, 1988.

(25) Skodje, R. T.; Truhlar, D. G.; Garrett, B. C. *J. Phys. Chem.* **1982**, *86*, 1136. Truhlar, D. G.; Isaacson, A. D.; Skodje, R. T.; Garrett, B. C. *J. Phys. Chem.* **1982**, *86*, 2252.

Table IV. Factor Analysis of the KIEs at 300 K

reaction	KIE	k_H/k_D	factors				
			η_κ	η_{trans}	η_{rot}	η_{vib}	η_{pot}
2. $Cl^- + CD_3Cl$	k_1/k_2	0.95	0.989	1.04	1.22	0.76	1.00
4. $Cl^-(H_2O) + CD_3Cl$	k_3/k_4	0.94	0.994	1.05	1.69	0.53	1.00
5. $Cl^-(D_2O) + CH_3Cl$	k_3/k_5	1.04	1.00	1.03	1.41	0.72	1.00
7. $Cl^-(H_2O)_2 + CD_3Cl$	k_6/k_7	0.91	0.985	1.05	1.71	0.51	1.00
8. $Cl^-(D_2O)_2 + CH_3Cl$	k_6/k_8	1.24	0.985	1.03	1.03	1.19	1.00

Analysis

In order to understand these results we carried out factor analyses[26,27] of the KIEs. In particular we note that[21,22]

$$k^{CVT/SCSAG} = \kappa^{SC}\frac{\sigma\tilde{k}T}{h}R_{trans}R_{rot}R_{vib}\exp(-V^{CVT}/N_A\tilde{k}T) \quad (2)$$

where σ is a symmetry factor, $\tilde{k}$ is Boltzmann's constant, T is temperature, h is Planck's constant, R_{trans} is the ratio of the translational partition function for the variational transition state to that for reactants, R_{rot} and R_{vib} are similar ratios for rotational and vibrational degrees of freedom, V^{CVT} is the molar potential energy at the variational transition state, and N_A is Avogadro's number. Noting that σ is independent of isotopic substitution for the cases considered in this article, the ratio of the rate constant for the undeuterated reaction to that for the deuterated one may be written as

$$k_H/k_D = \eta_\kappa\eta_{trans}\eta_{rot}\eta_{vib}\eta_{pot} \quad (3)$$

where

$$\eta_\kappa = \kappa_H^{SC}/\kappa_D^{SC} \quad (4)$$

$$\eta_X = R_{X,H}/R_{X,D}\ (X = \text{trans, rot, or vib}) \quad (5)$$

and

$$\eta_{pot} = \exp[-(V_H^{CVT} - V_D^{CVT})/N_A\tilde{k}T] \quad (6)$$

The results of the factor analysis at 300 K are shown in Table IV. This table shows clearly that the KIEs are usually dominated by vibrational effects, usually partly cancelled by an opposing rotational effect. The only exception to vibrational dominance occurs for the solvent KIE with one water (k_3/k_5), where rotational effects dominate. (However, the expression of KIE factors as percentages can be misleading since the normal rotational KIE effect of 41% is almost completely cancelled by the inverse vibrational effect of 28%.) The only case where rotational and vibrational effects do not partly cancel is k_6/k_8, where—unlike the other KIEs—the ratio η_{vib} is normal. Since the qualitative explanations of KIEs are usually based on vibrational effects, the factor analysis of Table IV provides a very important example of how such explanations can be misleading. Thus the vibrational effects are much larger for k_3/k_4 and k_6/k_7, about a factor of 2, than for k_6/k_8, about 20%, even though the net KIE is less than 10% for k_3/k_4 and k_6/k_7 but is 24% for k_6/k_8.

In order to achieve a more detailed understanding we further factor η_{vib} into contributions from individual vibrational modes. For reactant modes we write

$$\eta^R_{vib,m} = Q^R_{vib,m,D}/Q^R_{vib,m,H} \quad (7)$$

for each mode m, where $Q^R_{vib,m}$ is the vibrational partition function for mode m of reactants with zero of energy at the classical equilibrium geometry of reactants. For transition-state modes we write

$$\eta^{CVT}_{vib,m} = \frac{Q^{GT}_{vib,m,H}(s^{CVT}_{*,H})}{Q^{GT}_{vib,m,D}(s^{CVT}_{*,D})} \quad (8)$$

(26) Garrett, B. C.; Truhlar, D. G.; Magnuson, A. W. *J. Chem. Phys.* **1982**, *76*, 2321. Tucker, S. C.; Truhlar, D. G.; Garrett, B. C.; Isaacson, A. D. *J. Chem. Phys.* **1985**, *82*, 4102.

(27) Lu, D.-h.; Maurice, D.; Truhlar, D. G. *J. Am. Chem. Soc.* **1990**, *112*, 6206.

Table V. Harmonic Reactant Vibrational Frequencies (cm^{-1}) for Reaction with One Water

mode	$Cl^-(H_2O)$	$Cl^-(D_2O)$	CH_3Cl	CD_3Cl
1	3919	2860	3092	2295
2	3681	2673	3092	2295
3	1758	1281	2981	2134
4	603	438	1453	1051
5	269	194	1453	1051
6	132	126	1377	1044
7			1017	765
8			1017	765
9			741	703

Table VI. Harmonic Saddle Point Vibrational Frequencies (cm^{-1}) for Reaction with One Water

mode	$ClCH_3Cl(H_2O)^-$	$ClCD_3Cl(H_2O)^-$	$ClCH_3Cl(D_2O)^-$
1	3854	3854	3309
2	3751	3751	3307
3	3309	2472	3105
4	3307	2470	2823
5	3105	2196	2716
6	1701	1670	1394
7	1388	1023	1384
8	1384	1019	1234
9	1023	737	1023
10	950	674	950
11	948	672	948
12	422	450	312
13	363	363	259
14	328	328	232
15	231	228	231
16	211	197	211
17	206	189	206
18	113	91	112
19	92	83	88
20	47	47	46
21	584i	583i	584i

Table VII. Harmonic Reactant Vibrational Frequencies (cm^{-1}) for Reaction with Two Waters

mode	$Cl^-(H_2O)_2$	$Cl^-(D_2O)_2$	mode	$Cl^-(H_2O)_2$	$Cl^-(D_2O)_2$
1	3875	2828	9	486	350
2	3776	2759	10	457	329
3	3646	2647	11	266	196
4	3586	2607	12	254	185
5	1814	1321	13	179	165
6	1717	1251	14	135	130
7	787	567	15	80	78
8	728	532			

where $Q^{GT}_{vib,m}(s)$ is the vibrational partition function for mode m of the generalized transition state at a distance s along the reaction path with zero of energy at the minimum potential for that transition state, and $s = s_*^{CVT}$ is the variational location of the transition state. Then

$$\eta_{vib} = \prod_{m=1}^{3N-M}\eta^R_{vib,m}\prod_{m=1}^{3N-7}\eta^{CVT}_{vib,m} \quad (9)$$

where N is the total number of atoms and M is the number of translations and rotations of reactants (M equals 9 for $n = 0$ and 12 for $n = 1$ or 2).

Tables V–IX give the vibrational frequencies for all reactants and saddle point modes. Table X gives the factors of eqs 7–9.

Table VIII. Harmonic Saddle Point Vibrational Frequencies (cm^{-1}) for Reaction with Two Waters

mode	$ClCH_3Cl(H_2O)_2^-$	$ClCD_3Cl(H_2O)_2^-$	$ClCH_3Cl(D_2O)_2^-$
1	3860	3860	3308
2	3856	3856	3307
3	3755	3755	3104
4	3754	3754	2828
5	3308	2471	2825
6	3307	2470	2719
7	3104	2196	2718
8	1699	1698	1399
9	1689	1687	1392
10	1391	1024	1234
11	1389	1022	1223
12	1025	739	1024
13	952	676	952
14	950	674	950
15	413	413	302
16	395	387	300
17	361	361	257
18	357	356	254
19	324	325	235
20	315	315	230
21	235	234	223
22	219	201	219
23	204	190	204
24	153	112	148
25	90	90	87
26	86	86	82
27	44	44	43
28	43	43	42
29	22	22	22
30	669i	668i	669i

Table IX. Harmonic Saddle Point Frequencies for Reaction without Water

mode	$ClCH_3Cl^-$	$ClCD_3Cl^-$	mode	$ClCH_3Cl^-$	$ClCD_3Cl^-$
1	3309	2472	7	947	671
2	3309	2472	8	947	671
3	3106	2197	9	220	220
4	1381	1018	10	206	190
5	1381	1017	11	206	190
6	1021	735	12	469i	469i

The rows are labeled by reactant or saddle point frequencies (cm^{-1}) of the perprotio case with $n = 2$, i.e., reaction 6 in the convention used in the tables.

Since several of the modes with frequencies below 500 cm^{-1} cross and may interact strongly as the system progresses along the reaction path, their effects are multiplied together, i.e.

$$\eta_{vib,low} = \left(\prod_{m=M^R+1}^{3N-M} \eta^R_{vib,m}\right)\left(\prod_{m=M^{GT}+1}^{3N-M} \eta^{CVT}_{vib,m}\right)\left(\prod_{m=3N-M+1}^{3N-7} \eta^{CVT}_{vib,m}\right) \quad (10)$$

where N and M are as in eq 9, N^R is the number of atoms in the molecular reactant, M^R or M^{GT} is the number of modes of reactant or generalized transition state respectively with frequency above 500 cm^{-1}, the first two factors in (10) represent the overall contribution of low-frequency modes present in both the reactants and the generalized transition state, and the third factor is the overall contribution of transitory modes which do not correlate with bound vibrational modes or reactants. We also define the contribution of high-frequency modes as

$$\eta_{vib,high} = \left(\prod_{m=1}^{M'} \eta^R_{vib,m}\eta^{CVT}_{vib,m}\right) \quad (11)$$

where M' is the number of modes with frequencies above 2000 cm^{-1}. Finally the contribution of mid-frequency modes is defined by

$$\eta_{vib,mid} = \eta_{vib}/(\eta_{vib,low}\eta_{vib,high}) \quad (12)$$

This separation into three ranges of modes is well-defined because there are no modes of reactants or saddle point for any of the reactions 1–8 with frequencies in the range 487–531 cm^{-1} or in the range 1815–2133 cm^{-1}, only one mode moves from one of the three groups to another upon isotopic substitution (this mode, the 603-cm^{-1} mode of $Cl^-(H_2O)$, which decreases to 438 cm^{-1} upon isotopic substitution, is treated as a mid-frequency mode in the present analysis), and no modes move in or out of the high-frequency group as the system proceeds from reactants to the transition state. (Although the number of modes in the low- and mid-frequency ranges is not conserved, no modes which retain a recognizable character move from one group to another.) The high-frequency modes are C–H and O–H stretches, and the mid-frequency modes are CH_3 modes, the C–Cl stretch, and, for $n \neq 0$, water bends and some of the water librations. The three factors and their products are compared in Table XI.

Table X. Factorization of η_{vib} at 300 K[a]

mode	k_1/k_2	k_3/k_4	k_3/k_5	k_6/k_7	k_6/k_8
			CH_3Cl Modes ($\eta^R_{vib,m}$)		
3092	6.75	6.75	1.00	6.75	1.00
3092	6.75	6.75	1.00	6.75	1.00
2981	7.61	7.61	1.00	7.61	1.00
1453	2.64	2.64	1.00	2.64	1.00
1453	2.64	2.64	1.00	2.64	1.00
1377	2.23	2.23	1.00	2.23	1.00
1017	1.86	1.86	1.00	1.86	1.00
1017	1.86	1.86	1.00	1.86	1.00
741	1.10	1.10	1.00	1.10	1.00
			$Cl^-(H_2O)_n$ Modes ($\eta^R_{vib,m}$)		
3875		1.00	12.7	1.00	12.4
3776				1.00	11.5
3646		1.00	11.2	1.00	11.0
3586				1.00	10.5
1814				1.00	3.26
1717		1.00	3.14	1.00	3.06
787				1.00	1.77
728		1.00	1.60	1.00	1.68
under 500		1.00[b]	1.50[b]	1.00[c]	5.41[c]
			Generalized Transition State Modes ($\eta^{CVT}_{vib,m}$)		
3860				1.00	0.0838
3856		1.00	0.0842	1.00	0.0846
3755				1.00	0.0837
3754		1.00	0.0838	1.00	0.0831
3308	0.135	0.135	1.00	0.134	1.00
3307	0.135	0.135	1.00	0.135	1.00
3104	0.113	0.113	1.00	0.113	1.00
1699		0.994	0.325	0.994	0.327
1689				0.994	0.326
1391	0.416	0.415	1.01	0.413	1.02
1389	0.416	0.415	1.00	0.413	1.01
1025	0.492	0.492	1.00	0.492	0.999
952	0.500	0.502	1.00	0.500	1.00
950	0.500	0.500	1.00	0.502	1.00
under 500	0.846[d]	0.596[e]	0.290[e]	0.589[f]	0.0830[f]

[a] Calculated from eq 7 for reactant modes and eq 8 for the modes of the generalized transition state. [b] Two modes. [c] Seven modes. [d] Three modes. [e] Nine modes. [f] Fifteen modes.

Table XI. Factorization of η_{vib} at 300 K for Correlated and Transitory Modes

reaction	KIE	η_{vib}	factors		
			$\eta_{vib,low}$	$\eta_{vib,mid}$	$\eta_{vib,high}$
2. $Cl^- + CD_3Cl$	k_1/k_2	0.76	0.85	1.26	0.71
4. $Cl^-(H_2O) + CD_3Cl$	k_3/k_4	0.53	0.60	1.25	0.71
5. $Cl^-(D_2O) + CH_3Cl$	k_3/k_5	0.72	0.43	1.65	1.00
7. $Cl^-(H_2O)_2 + CD_3Cl$	k_6/k_7	0.51	0.59	1.23	0.71
8. $Cl^-(D_2O)_2 + CH_3Cl$	k_6/k_8	1.19	0.45	3.25	0.81

Although, of course, the higher frequency modes give larger effects when we look at reactants and transition states separately, as in Table X, this would not necessarily imply that these modes make the largest contributions to the KIE since there is considerable cancellation of these contributions. Table XI shows in fact that for k_1/k_2 the net effect of high-frequency modes nearly cancels for one of the solvent KIEs, is 19% for the other, and is 29% for the unhydrated and microhydrated CH_3/CD_3 effects.

For the unhydrated CH_3/CD_3 kinetic isotope effect, Tables IV and XI show that the 29% effect of the high-frequency modes is the single factor most responsible for the inverse KIE. This effect receives additional support from a 15% inverse contribution due to low-frequency modes, and it is opposed primarily by a 22% normal effect due to rotations and a 26% normal effect due to mid-frequency modes. The other modes (translation and the reaction coordinate) make a cumulative contribution of only 2%.

Next consider the effect of adding a single solvent molecule on the secondary KIE corresponding to substitution of CH_3 by CD_3. The rough constancy of this KIE, 0.94 for $n = 1$ vs 0.95 for $n = 0$, is due to a significant decrease in the vibrational contribution; otherwise the increasing rotational contribution (see Table IV, 1.69 vs 1.22) would change the KIE to normal. The overall vibrational factor for k_3/k_4 is 0.53 as compared to 0.76 for k_1/k_2. Clearly, from Tables X and XI, this change results mainly from a change in the low-frequency modes of the transition states. In fact the effect of microhydration on the secondary KIE is traceable almost entirely to a single transition-state mode, the twist of CH_3 or CD_3 around the Cl–Cl axis. The twist mode is a rotation in the absence of solvent, but the presence of water converts it into a low-frequency vibration. This mode also dominates the change of the KIE from k_1/k_2 to k_6/k_7 when one more solvent molecule is added. This mode has frequencies of 113, 91, 152, and 112 cm^{-1} for reactions 3, 4, 6, and 7, respectively.

Now consider the solvent KIEs. Reactions 5 and 8 involve deuterium substitution in the solvent. The overall vibrational contributions for these reactions are not simple—for k_3/k_5, η_{vib} is inverse, but for k_6/k_8, it is normal. The change of the vibrational contribution from inverse to normal by adding one more solvent molecule is due to mid-frequency modes; their contribution varies from 1.65 for k_3/k_5 to 3.25 for k_6/k_8 (see Table XI). In this case the effect can be traced almost entirely to two modes, both water librational modes of the solvated Cl^- reactant. One, at 787 cm^{-1}, corresponds to an out-of-plane bend of the water–water hydrogen bond[28] (see Figure 1), and the other, at 728 cm^{-1}, corresponds to the water–Cl^- bending motion. This is a good example of an initial-state effect since both modes correlate adiabatically with very different lower frequency transition-state modes that are less isotopically sensitive.

One important question answered by the above analysis is whether the solvent KIE is rotational, direct vibrational, or indirect vibrational. An indirect vibrational effect would be associated with isotopic substitution in the solvent changing the solute vibrational frequencies by mode mixing. A direct effect is associated with modes in which the solvent participates directly, e.g., stretching of the $Cl^-\cdots HOH$ solvation coordinate. The above discussion and Table IV show that the normal solvent KIE for $n = 1$ is attributable to a rotational effect, and the increase for $n = 2$ is primarily an initial-state direct vibrational effect.

Discussion

α-Deuterium Substitution. The conventional interpretation of α-deuterium secondary KIEs focuses on the hybridization at the α-carbon.[29-38] When this is changing from sp^3 to sp^2, as in S_N2 reactions, one would "ordinarily" expect a normal KIE for $N^- + CH_3X$ due to a decrease in H–C–H and H–C–X bending force constants in proceeding from reactant to transition state, although there is some counterbalancing by increasing N–C–H bending force constants. Most quantitative discussions of α-deuterium secondary KIES on S_N2 or S_N1 reactions have focussed on leaving group participation in and influence on CH_3 deformation modes affected by such force constants. In fact α-deuterium KIEs on bimolecular substitution reactions at methyl are typically inverse,[38-40] with values reported as low as 0.87,[30] but are sometimes normal, with values as large as 1.10 reported.[32] (The "experimental" value for the present reaction is inferred by a Marcus theory analysis to be 0.97.[39]) The inverse effects have been interpreted as indicating that "the bending motion of the α-hydrogen may be more constrained in an S_N2 transition state than in the reactant",[36] but it has also been stated that, even when the KIE is inverse, "the information given by k_H/k_D is clear" and "a larger k_H/k_D indicates a transition state in which the out-of-plane bend of the α-hydrogen is less encumbered than in the reactant".[38] The Arrhenius parameters of the KIE are also sensitive to the C–H stretching force constant.[33]

The analysis presented in the previous section provides an ab initio test of the conventional model for k_H/k_D values and whether these result primarily from the out-of-plane bend (i.e., the umbrella mode of the transition state), the H–C–H bends, or the C–H stretch. The CH_3 deformations (including the H–C–H bends and the umbrella mode) are modes 4–8 at the $n = 0$ transition state, 7–11 at the $n = 1$ transition state, 10–14 at the $n = 2$ transition state, and 4–8 in CH_3Cl. Multiplying the mode-specific KIEs (i.e., the $\eta_{vib,m}^{CVT}$ and $\eta_{vib,R}^{R}$ factors of Table X) for these modes yields 1.14 for k_1/k_2 and k_3/k_4 and 1.13 for k_6/k_7. Thus these modes actually contribute to a normal KIE, which follows from the fact that they all decrease in frequency. The C–H stretches are modes 1–3 for the transition states with $n = 0$, 3–5 for $n = 1$, 5–7 for $n = 2$, and 1–3 for CH_3Cl. Multiplying the six corresponding mode-specific KIEs yields 0.71 for all three reactions (see Table XI). As a result the C–H stretches are the dominant contributor to the inverse α-deuterium KIEs for the unhydrated S_N2 reaction, and they contribute almost as much as the cumulative effect of all low-frequency modes for the microhydrated cases (again see Table XI). In all three cases, if we simply omitted the contribution of the C–H stretches, the net KIE would be normal rather than inverse. Inverse KIEs result from isotopically sensitive vibrational modes that increase in frequency, in proceeding from reactants to the variational transition state, which the C–H stretches do in the ab initio calculations on which our potential energy function is based. In particular the scaled ab initio frequencies for the C–H stretches increase by 125–217 cm^{-1} in proceeding from the reactants to the transition state.[14] This increase is consistent with the transition state H—C(sp^2) bonds being stronger than the reactant H—C(sp^3) bonds, and it implies that C—H bonds in $R_2C{=}CRH$ systems are a better model than those in O=CRH systems for the C—H bonds at the present transition state.

The only other α-deuterium KIEs studied by variational transition-state theory are the reactions $CH_4/CD_3H + H/D \rightarrow CH_3/CD_3 + H_2/HD$.[27] In these cases, in addition to large tunneling effects, there was a very significant difference in the overbarrier KIE between the variational and conventional transition-state calculations. In the present case, in contrast, the variational and tunneling effects on the KIE are negligible. Nevertheless there are also similarities between these two cases. The C–H stretches, for example, contribute an inverse factor of 0.70 at the level of conventional transition-state theory, although they contribute a normal factor of 1.18 to k_H/k_D in the canonical variational calculation for the $CH_4/CD_3H + H \rightarrow H_2 + CH_3/CD_3$ case. As a result the best estimate of the non-tunneling α-deuterium secondary KIE is 1.22, so again the stretches are very important in determining the overall effect.

(28) This mode also occurs in the isolated water dimer as analyzed by: Reimers, J. R.; Watts, R. O. *Chem. Phys.* **1984**, *85*, 83. In the notation of that reference it is ν_{10}.
(29) Streitweiser, A., Jr.; Jagow, R. H.; Fahey, R. C.; Suzuki, S. *J. Am. Chem. Soc.* **1958**, *80*, 2326.
(30) Llewellyn, J. A.; Robertson, R. E.; Scott, J. W. M. *Can. J. Chem.* **1960**, *38*, 222.
(31) Weston, R. E., Jr. *Annu. Rev. Nucl. Sci.* **1961**, *11*, 439.
(32) Seltzer, S.; Zavitsas, A. A. *Can. J. Chem.* **1967**, *45*, 2023.
(33) Willi, A. V.; Won, C. M. *J. Am. Chem. Soc.* **1968**, *90*, 5999.
(34) Scheppele, S. E. *Chem. Rev.* **1972**, *72*, 511.
(35) Buddenbaum, W. E.; Shiner, V. J., Jr. In *Isotope Effects on Enzyme Catalyzed Reactions*; Cleland, W. W., O'Leary, M. H., Northrup, D. B., Eds.; University Park Press: Baltimore, 1977; p 1.
(36) Melander, L.; Saunders, W. H. *Reaction Rates of Isotopic Molecules*; Wiley: New York, 1980.
(37) Yamataka, H.; Tamura, S.; Hanafusa, T.; Ando, T. *J. Am. Chem. Soc.* **1985**, *107*, 5429.
(38) Saunders, W. H., Jr. In *Investigation of Rates and Mechanisms of Reactions*, 4th ed., Part I; Bernasconi, C. F., Ed.; Wiley: New York, 1986; p 565.
(39) Albery, W. J.; Kreevoy, M. M. *Adv. Phys. Org. Chem.* **1978**, *16*, 87.
(40) Thornton, E. R. *Annu. Rev. Phys. Chem.* **1966**, *17*, 349.

Solvent KIEs. Aqueous solvent KIEs have been extensively analyzed for reactions involving exchangeable protons, and they reflect the fractionation of D into the solute and transition state relative to water. Solvent KIEs that reflect nonreactive solvation effects have also been studied, but they are harder to analyze.[31,40-43] The microsolvent KIEs on reactions 3 and 6 are of the latter type. Since our solvent–solute coupling potential is not as reliable as our solute force field, our results for the microsolvent KIEs are correspondingly more uncertain as well. Nevertheless we believe that this kind of calculation leads to interesting insight into the factors which must be considered in interpreting microsolvent KIES, and we hope they provide a stimulus for measuring these effects as a way to test force fields that might also be used to study bulk solvent KIEs. In addition it would be interesting to test the sensitivity of the present result for the cluster microsolvent KIE with $n = 2$ to improvements in the potential energy functions for the water interactions.

One possible source of solvent KIEs in S_N2 reactions is solvent reorganization at sites of changing charge character.[39-41,44] Another, partly equivalent, possibility is the change in frequencies of librational degrees of freedom of the water molecules as reaction progresses.[45]

On the basis of earlier work by Swain and Bader,[45] Schowen[42] has proposed a simple method for solvent KIEs of hydrolysis reactions. These workers modeled the solvent KIE in terms of the effect of ionic charges on water librations, assuming, in good accord with more recent studies,[46] that the water-structure-breaking effect of a solute is dominated by the first hydration shell, in which water is held more loosely than in the absence of solute. In this model, since we are proceeding to a transition state in which charge is more dispersed than in reactants, the water structure will be strengthened in the transition state, and the kinetic isotope effect will be inverse. Schowen assumes that each inner-sphere water of hydration contributes a factor of $(1.5)^{(|q^*|-|q^R|)/4}$ to k_H/k_D, where q^* is the charge solvated in the transition state, and q^R is the charge solvated in the reactants. In the cases considered here, $|q^R|$ is unity, but $|q^*|$ is unclear since the water is bridging the whole delocalized charge distribution consisting of two chlorides, each with $q = -0.7$, and the methyl group, with $q = +0.4$. If the perturbation of water structure by the charge-delocalized transition state were less than that by the localized charge in reactants, one would calculate by this model that $(1.5)^{-2/4} \leq k_H/k_D \lesssim 1$ for $n = 2$, which yields 0.82–1.00. This can be compared to the present results for the product $\eta_{vib,low}\eta_{vib,mid}$, which equals 1.46 for k_6/k_8. Clearly, as seen in Table X and discussed above, many modes contribute to the solvent KIE in the present case, and this bulk water model is not applicable to the microhydrated reactions studied here. In fact, even though charge is dispersed in proceeding to the transition state, we find normal rather than inverse solvent KIEs for the present potential energy function and dynamics treatment. This is consistent with the fact that for the microhydrated reactant with $n = 2$, there is actually more water structure breaking at the transition state, where the water dimer hydrogen bond is broken, than for the reactant, where it is not.

In liquid water the differences in water–water modes between the reactant and the transition state may be quite different than observed here where a water–water hydrogen bond is fully broken in proceeding to the transition state. In both microhydrated reactions and bulk water the solvent kinetic isotope effect may give unique information about such water-structure breaking at reactants and transition states.

Concluding Remarks

We have seen that the origins of kinetic isotope effects for microhydrated reactions can be understood in intimate detail. Rotations and identifiable vibrational modes are found to be very important. The inverse α-deuterium KIE for the unhydrated S_N2 reactions at methyl is attributable to C–H stretches, whose role is neglected in most previous models, and not to tightening of the CH_3 deformations. The C–H stretches also make a critical contribution to the inverse α-deuterium KIE for the microhydrated S_N2 reactions with one or two water molecules, and one would assume that this C–H stretch effect is also very important for reactions in solution. The solvent KIE is attributable to the CH_3 internal rotation around the Cl–Cl axis for the case of solvation by one water and to H_2O librations in the initial state for the case of two waters. In bulk solution the solvent KIEs may be dominated by other motions since in bulk solution the solvent molecules are not expected to carry out the large-scale migrations observed in the microhydrated gas-phase reactions. Nevertheless it is quite interesting that the widely discussed phenomenon of solvent structure breaking plays an important role at the transition state of the microhydrated reaction with the absolute minimum number, two, of solvent molecules required for it to be possible. Experimental measurements of the solvent KIEs for microhydrated reactions would provide a very challenging test for solvation force fields.

Acknowledgment. The authors are grateful to M. M. Kreevoy and Angels Gonzalez-Lafont for discussions of many relevant issues. This work was supported in part by the U.S. Department of Energy, Office of Basic Energy Sciences and a graduate fellowship to X. G. Zhao supported by Air Products Foundation.

(41) Laughton, P. M.; Robertson, R. E. In *Solvent Isotope Effects for Equilibria and Reactions*; Coetzee, J. F., Ritchie, C. D., Eds.; Marcel Dekker: New York, 1969; p 399.
(42) Schowen, R. L. *Prog. Phys. Org. Chem.* **1972**, *9*, 275.
(43) Blandamer, M. J.; Burgess, M.; Clare, N. P.; Duce, P. P.; Gray, R. P.; Robertson, R. E.; Scott, J. W. M. *J. Chem. Soc., Faraday Trans. 1* **1982**, *78*, 1103. Blandamer, M. J.; Burgess, J.; Robertson, R. E.; Koshy, K. M.; Ko, E. C. F.; Golinkin, H. S.; Scott, J. M. W. *J. Chem. Soc., Faraday Trans. 1* **1984**, *80*, 2287.
(44) Swain, C. G.; Thornton, E. R. *J. Am. Chem. Soc.* **1962**, *84*, 822.
(45) Swain, C. G.; Bader, R. F. W. *Tetrahedron* **1960**, *10*, 182, 200.
(46) Collins, K. D.; Washabaugh, M. W. *Q. Rev. Biophys.* **1985**, *18*, 323.

photoelectron data suggest that the weakly bound butadiene state does not interact significantly with the molybdenum surface since it has a rather high C(1s) binding energy (~285 eV). Butadiene directly bound to the surface is expected to have a lower C(1s) binding energy due to final state screening. Interestingly, ethylene sulfide deposits 0.32 monolayer of sulfur during reaction, compared to 0.23 for 2,5-DHT and ~0.1 for tetrahydrothiophene and thiophene. Consistent with this explanation, in the case of ethylene sulfide, ethylene is directly evolved into the gas phase at 100 K so that the product does not occupy surface sites. In contrast, both tetrahydrothiophene and thiophene initially form strongly bound products.

The marked dependence of the reaction selectivity on the initial exposure of 2,5-dihydrothiophene (Figure 3) may be caused by a modification of the surface activity as the coverage of reaction products, such as sulfur and/or hydrocarbon fragments, increases. In experiments explicitly examining the effects of surface sulfur on desulfurization reactions, the presence of adsorbed sulfur was found to slow the kinetics for nonselective reaction of both sulfur-containing and hydrocarbon reaction intermediates on Mo(110).[32] A similar effect is proposed here since we have shown experimentally that some nonselective reaction occurs upon adsorption at 120 K. Since this process is apparently not reversible, postulated changes in adsorbate structure induced by intermolecular interactions at high coverage, thought to be important in the reactions of large thiols on Mo(110),[19] are not necessary for explaining coverage-dependent selectivities in the case of 2,5-dihydrothiophene.

The presence of *molecular* 2,5-dihydrothiophene on the surface also appears to modify the kinetics for butadiene elimination. A pronounced maximum in the rate of butadiene evolution is observed just above the 2,5-DHT desorption peak near 210 K for large initial 2,5-DHT exposures (relative exposure > 0.8) (Figure 1). The coincidence of a maximum in the rate of butadiene elimination with the trailing edge of 2,5-DHT desorption suggests that 2,5-dihydrothiophene modifies its own reaction kinetics either through effects on the local electronic structure or by site blocking.

Conclusions. 2,5-Dihydrothiophene readily eliminates butadiene during temperature-programmed reaction on Mo(110). Approximately two-thirds of the irreversibly adsorbed 2,5-DHT yields gaseous butadiene and adsorbed sulfur via an intramolecular elimination process, while one-third is nonselectively decomposed on the surface without producing any gas-phase hydrocarbons. Selective desulfurization to form gaseous butadiene is favored at high initial 2,5-DHT coverages, possibly because of a moderation of the surface activity as decomposition products, such as sulfur, are deposited during reaction. The differences between the reactivity of 2,5-DHT and those of thiophene and tetrahydrothiophene are attributed largely to the fact that intramolecular elimination is kinetically more favorable for 2,5-DHT. Only minimal reorganization is required along the path for butadiene formation from 2,5-DHT, while thiophene has no stable gaseous elimination product and cyclobutane formation from tetrahydrothiophene would require substantial displacement of the carbons bound to the sulfur. These findings are generally consistent with previous studies of 2,5-DHT reactivity on high surface area catalysts and in organometallic complexes.

Acknowledgment. The 2,5-dihydrothiophene used in these experiments was kindly provided by Prof. R. J. Angelici of Iowa State University and was synthesized by Moon-Gun Choi. Funding for this research was provided by the Department of Energy, Basic Energy Sciences, Grant DE-FG02-84ER13289.

(32) Wiegand, B. C.; Roberts, J. T.; Friend, C. M. Unpublished results.

Solvent and Secondary Kinetic Isotope Effects for the Microhydrated S_N2 Reaction of $Cl^-(H_2O)_n$ with CH_3Cl

Xin Gui Zhao, Susan C. Tucker,† and Donald G. Truhlar*

Contribution from the Department of Chemistry, Chemical Physics Program, and Supercomputer Institute, University of Minnesota, Minneapolis, Minnesota 55455-0431. *Received May 21, 1990. Revised Manuscript Received September 27, 1990*

Abstract: We have calculated gas-phase rate coefficients and deuterium kinetic isotope effects (KIEs) for isotopic substitution in either the methyl group or the water of the title reaction with $n = 1$ and 2. The calculations are carried out by variational transition-state theory with semiclassical transmission coefficients, and they are based on 27- and 36-dimensional reaction-path potentials presented previously. A critical aspect of the potentials is that the solute part is based on high-level ab initio calculations. We also analyze the effect of deuterium substitution at methyl for the case of $n = 0$. We calculate an inverse effect for substitution at methyl both for bare solute ($n = 0$) and for microhydrated solute with $n = 1$ or 2. A detailed mode analysis shows that the inverse effect for the unhydrated reaction is dominated by C-H stretch contributions rather than by CH_3 deformations as is usually assumed in analyzing experimental data on solution-phase reactions. Furthermore, the C-H stretch contribution to the inverse α-deuterium KIE is essentially unaffected by microhydration. We find that for $n = 1$ the secondary KIE for substitution at methyl is larger than the solvent KIE, but for $n = 2$ the trend is reversed. The solvent KIEs are also interpreted in terms of the contributions of individual vibrational modes; in the $n = 2$ case the KIE is attributable to the breaking of a water-water hydrogen bond and the weakening of a water-chloride hydrogen bond.

Introduction

Gas-phase reactions of microhydrated ions provide opportunities for exploring fundamental concepts of condensed-phase kinetics using the techniques, both experimental and theoretical, of few-body gas-phase dynamics.[1-12] In previous work[12] we have cal-

* Author to whom correspondence should be addressed.
† Current address: Department of Chemistry, Columbia University, New York, NY 10027.

(1) Fehsenfeld, F. C.; Ferguson, E. E. *J. Chem. Phys.* **1974**, *61*, 3181. Fehsenfeld, F. C.; Dotan, I.; Albritton, D. L.; Howard, C. J.; Ferguson, E. E. *J. Geophys. Res.* **1978**, *33*, 1333. Bohringer, H.; Fahey, D. W.; Fehsenfeld, F. C.; Ferguson, E. E. *Planet Space Sci.* **1983**, *31*, 185.

0002-7863/91/1513-826$02.50/0

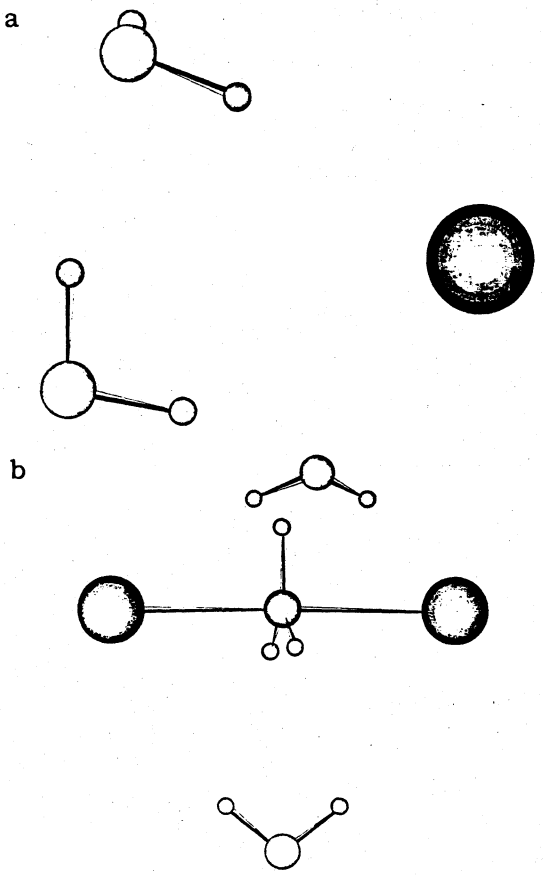

Figure 1. (a) Structure of $Cl^-(H_2O)_2$. (b) Structure of $Cl{-}CH_3{-}Cl^-(H_2O)_2$ at the saddle point.

culated the variational transition-state-theory rate constant for the reactions

$$Cl^-(H_2O)_n + CH_3Cl' \rightarrow ClCH_3 + Cl'^-(H_2O)_n \quad (R1)$$

with n = 0, 1, and 2 and for

$$Cl^-(H_2O)_n + CD_3Cl' \rightarrow ClCD_3 + Cl'^-(H_2O)_n \quad (R2)$$

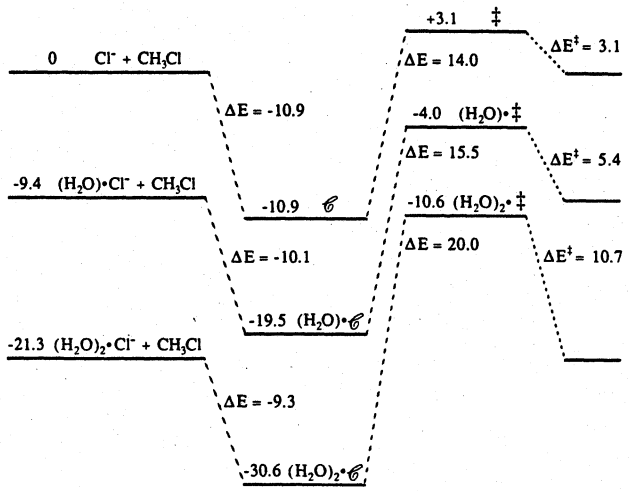

Figure 2. Reaction energetics, in kcal/mol on an energy scale having the zero of energy at infinitely separated $H_2O + H_2O + Cl^- + CH_3Cl$, for reaction R2 with n = 0, 1, and 2. For all reactions the ion–dipole complex on the product side has been omitted from the diagram since its energy is identical with that of the reactant-side complex.

with n = 0. A major focus of that work was to test the hypothesis of "equilibrium solvation". In the present paper we focus on kinetic isotope effects (KIEs) for such microsolvated reactions, and we extend the previous calculations to include reaction R2 with n = 1 and 2 and the reaction

$$Cl^-(D_2O)_n + CH_3Cl' \rightarrow ClCH_3 + Cl'^-(D_2O)_n \quad (R3)$$

also with n = 1 and 2. These calculations are used to gain insight about the coupling of solutes to first-hydration-shell molecules in charge migration reactions. In addition, since such gas-phase cluster ion reactions are of great experimental[1-7] interest, we hope that our predictions will be tested experimentally.

Methods

The dynamical calculations involve three steps: (i) choice of potential energy function, (ii) variational transition-state-theory calculations with quantized vibrations and classical rotational and reaction-coordinate motions, and (iii) inclusion of tunneling effects by a multidimensional semiclassical ground-state transmission coefficient.

(i) The potential energy function for the present study is taken from previous work[12] by two of the authors. In particular, for n = 0, it is a semiglobal analytic representation of ab initio electronic structure calculations at the MP2/6-31G(d,p) level[13,14] with empirical adjustment of the saddle point height to the experimental rate constant of Barlow et al.[15] For $n > 0$ the water and water–dimer potential are based[12] on the work of Watts and co-workers,[16] and the water–solute interactions are included[12] by using atom–atom potential parameters developed by Clementi and co-workers,[17] plus charge–charge interactions. All degrees of freedom are treated as nonrigid, giving 18, 27, and 36 degrees of freedom for n = 0, 1, and 2, respectively.

The resulting potential function for n = 0 has a classical binding energy of 11.0 kcal/mol for the ion–dipole complex and a 3.1 kcal/mol symmetric barrier with respect to reactants (14.1 kcal/mol with respect to the precursor and successor complexes.) Adding one or two water molecules increases the barrier with respect to reactants to 5.4 and 10.7 kcal/mol, respectively. The first water of hydration forms a hydrogen bond to Cl^- in reactants and bridges the CH_3 group (between two C–H bonds) to form partial hydrogen bonds to both partially charged chlorides at the transition state. The solvation structure of the reactant and the

(2) Bohme, D. K.; Mackay, G. I.; Tanner, S. D. *J. Am. Chem. Soc.* **1979**, *101*, 3724. Tanner, S. D.; Mackay, G. I.; Bohme, D. K. *Can. J. Chem.* **1981**, *59*, 1615. Bohme, D. K.; Mackay, G. I. *J. Am. Chem. Soc.* **1981**, *103*, 978. Bohme, D. K.; Rakshit, A. B.; Mackay, G. I. *J. Am. Chem. Soc.* **1982**, *104*, 1100. Bohme, D. K.; Raksit, A. B. *J. Am. Chem. Soc.* **1984**, *106*, 3447; *Can. J. Chem.* **1985**, *63*, 3007.

(3) Smith, D.; Adams, N. G.; Henchman, M. J. *J. Chem. Phys.* **1980**, *72*, 4951. Henchman, M.; Paulson, J. F.; Hierl, P. M. *J. Am. Chem. Soc.* **1983**, *105*, 5509. Henchman, M.; Hierl, P. M.; Paulson, J. F. *J. Am. Chem. Soc.* **1985**, *107*, 2812. Hierl, P. M.; Ahrens, A. F.; Henchman, M.; Viggiano, A. A.; Paulson, J. F. *J. Am. Chem. Soc.* **1986**, *108*, 3140, 3142. Henchman, M.; Hierl, P. M.; Paulson, J. F. *ACS Adv. Chem. Ser.* **1987**, *215*, 83. Hierl, P. M.; Ahrens, A. F.; Henchman, M. J.; Viggiano, A. A.; Paulson, J. F.; Clary, D. C. *Faraday Discuss. Chem. Soc.* **1988**, *85*, 37.

(4) Caldwell, G.; Rozeboom, M. D.; Kiplinger, J. P.; Bartmess, J. E. *J. Am. Chem. Soc.* **1984**, *106*, 809.

(5) Lane, K. R.; Squires, R. R. *J. Am. Chem. Soc.* **1986**, *108*, 7187.

(6) Kebarle, P.; Dillow, G. W.; Hirao, K.; Chowdhury, S. *Faraday Discuss. Chem. Soc.* **1988**, *85*, 23.

(7) Baer, S.; Stoutland, P. O.; Brauman, J. I. *J. Am. Chem. Soc.* **1989**, *111*, 4097.

(8) Cremaschi, P.; Gamba, A.; Simonetta, M. *Theor. Chim. Acta* **1972**, *25*, 237.

(9) Morokuma, K. *J. Am. Chem. Soc.* **1982**, *104*, 3732. Ohta, K.; Morokuma, K. *J. Phys. Chem.* **1985**, *89*, 5845.

(10) Jaume, J.; Lluch, J. M.; Oliva, A.; Bertrán, J. *Chem. Phys. Lett.* **1984**, *106*, 232. Bertrán, J. In *New Theoretical Concepts for Understanding Organic Reactivity*; Bertrán, J., Csizmadia, I. G., Eds.; Kluwer: Dordrecht, 1989; p 291.

(11) Kong, Y. S.; Jhon, M. S. *Theor. Chim. Acta* **1986**, *70*, 123.

(12) Tucker, S. C.; Truhlar, D. G. *J. Am. Chem. Soc.* **1990**, *112*, 3338, 3347. Note that in this reference the KIE is discussed in terms of k_D/k_H whereas here we use the more standard k_H/k_D convention throughout.

(13) Hehre, W. J.; Radom, L.; Schleyer, P. v. R.; Pople, J. A. *Ab Initio Molecular Orbital Theory*; Wiley: New York, 1986.

(14) Tucker, S. C.; Truhlar, D. G. *J. Phys. Chem.* **1989**, *93*, 8138.

(15) Barlow, S. E.; Van Doren, J. M.; Bierbaum, V. M. *J. Am. Chem. Soc.* **1988**, *110*, 7240.

(16) Reimers, J. R.; Watts, R. O.; Klein, M. L. *Chem. Phys.* **1982**, *64*, 95. Reimers, J. R.; Watts, R. O. *Mol. Phys.* **1984**, *52*, 357. Coker, D. F.; Miller, R. E.; Watts, R. O. *J. Chem. Phys.* **1985**, *82*, 3554.

(17) Kistenmacher, H.; Popkie, H.; Clementi, E. *J. Chem. Phys.* **1973**, *59*, 5842. Clementi, E.; Cavallone, F.; Scordamaglia, R. *J. Am. Chem. Soc.* **1977**, *99*, 5531.

Table I. Rate Constants (cm^3 $molecule^{-1}$ s^{-1}) and Kinetic Isotope Effects at 300 K As Calculated by Conventional Transition-State Theory (‡), Improved Canonical Variational Theory (CVT), and Canonical Variational Theory Corrected for Tunneling (CVT/SCSAG)

	‡		CVT		CVT/SCSAG	
reaction	k	k_H/k_D	k	k_H/k_D	k	k_H/k_D
1. $Cl^- + CH_3Cl$	2.36×10^{-14}		2.28×10^{-14}		3.58×10^{-14}	
2. $Cl^- + CD_3Cl$	2.46×10^{-14}	0.96	2.38×10^{-14}	0.96	3.78×10^{-14}	0.95
3. $Cl^-(H_2O) + CH_3Cl$	6.38×10^{-18}		6.27×10^{-18}		1.09×10^{-17}	
4. $Cl^-(H_2O) + CD_3Cl$	6.73×10^{-18}	0.95	6.62×20^{-18}	0.95	1.15×10^{-17}	0.94
5. $Cl^-(D_2O) + CH_3Cl$	6.15×10^{-18}	1.04	6.04×10^{-18}	1.04	1.05×10^{-17}	1.04
6. $Cl^-(H_2O)_2 + CH_3Cl$	2.07×10^{-20}		2.05×10^{-20}		3.70×20^{-20}	
7. $Cl^-(H_2O)_2 + CD_3Cl$	2.23×10^{-20}	0.93	2.21×10^{-20}	0.93	4.05×10^{-20}	0.91
8. $Cl^-(D_2O)_2 + CH_3Cl$	1.65×10^{-20}	1.26	1.63×10^{-20}	1.26	2.99×10^{-20}	1.24

saddle point for $n = 2$ are shown in Figure 1; the structures for $n = 1$ are similar but with one water missing. Notice the presence of a water–water hydrogen bond in $Cl^-(H_2O)_2$ but not in the transition state.

(ii) Variational transition-state-theory[18-22] (VTST) calculations are carried out by canonical variational theory[19-21] (CVT) with quantized harmonic vibrations. (Improved canonical variational transition-state-theory[20,21] calculations were also carried out in all cases, and they gave essentially the same results. Thus we present only the simpler CVT calculations.) CVT involves first calculating the isotope-dependent minimum energy reaction path and the free energy of activation profile[20] as a function the displacement s along the reaction path and then locating the variational transition state at the maximum of this profile. For comparison with the CVT rate constant, denoted $k^{CVT}(T)$, we also calculated the rate constant by conventional transition-state theory,[21-23] and this result is denoted $k^{\ddagger}(T)$. We use the POLYRATE program,[24] developed in our laboratory, for both sets of calculations. We do *not* assume equilibrium solvation but rather we treat all degrees of freedom of both solute and solvent in the same footing without this additional assumption.

(iii) The final VTST rate constant is given by

$$k^{CVT/SCSAG}(T) = \kappa^{SC}(T)k^{CVT}(T) \quad (1)$$

where $\kappa^{SC}(T)$ is a transmission coefficient[20,21] calculated by the Small–Curvature Semiclassical Adiabatic Ground-State[21,25] method. This transmission coefficient corrects the theory for quantal effects on the reaction-coordinate motion, especially tunneling.

All calculations were converged with respect to numerical parameters to the full number of significant figures shown in the tables, and kinetic isotope effects were calculated from unrounded results. After the saddle point was located by the Newton–Raphson method, the reaction path along the minimum-energy path (MEP) was computed by following the negative of the gradient of the potential, in a mass-scaled coordinate system[20] with $\mu = 1$ amu, from the saddle point to the reactant and from the saddle point to the product. In all of our calculations, the negative gradient was followed using an Euler single-step integrator with a step size δs of 5×10^{-5} a_0 for the first 2000 steps in each direction and then a step size of 10^{-3} a_0. At intervals of 5×10^{-3} a_0 (reactions 1 and 2) or 10^{-2} a_0 (reactions 3–8) along the reaction paths, the hessian matrix of quadratic force constants was computed to obtain the generalized normal mode frequencies, the reaction path curvature, and the ground-state vibrationally adiabatic potential. Then, at the same intervals, the free energy of activation profile was evaluated and interpolated to get the generalized transition-state rate constants. The tunneling correction was evaluated using repeated Kronrod quadrature for both the $\theta(E)$ integral over s (eq 94 of ref 21) and the Boltzmann average (eq 91 of ref 21). The ranges of the integrals were divided into two equal segments and 61-point (reactions 1 and 2) or 81-point (reactions 3–8) Kronrod quadrature was used in each segment for both the $\theta(E)$ integral and the Boltzmann integral. The calculations were carried out on the Cray X-MP/4-16 computer at the Minnesota Supercomputer Institute.

Table II. Kinetic Isotope Effects k_H/k_D as Functions of Temperature (CVT/SCSAG)

		T (K)				
reaction	KIE	200	300	400	600	1000
2. $Cl^- + CD_3Cl$	k_1/k_2	0.91	0.95	0.95	0.94	0.96
4. $Cl^-(H_2O) + CD_3Cl$	k_3/k_4	0.90	0.94	0.95	0.95	0.96
5. $Cl^-(D_2O) + CH_3Cl$	k_3/k_5	1.04	1.04	1.03	1.02	1.01
7. $Cl^-(H_2O)_2 + CD_3Cl$	k_6/k_7	0.85	0.91	0.93	0.94	0.95
8. $Cl^-(D_2O)_2 + CH_3Cl$	k_6/k_8	1.55	1.24	1.12	1.03	0.99

Table III. Arrhenius Preexponential Factor A (cm^3 $molecule^{-1}$ s^{-1}) and Activation Energy (kcal/mol) at 300 K[a] from CVT/SCSAG Calculations

reaction	A	E_a
1. $Cl^- + CH_3Cl$	5.21×10^{-12}	2.97
2. $Cl^- + CD_3Cl$	5.33×10^{-12}	2.95
3. $Cl^-(H_2O) + CH_3Cl$	2.56×10^{-13}	6.00
4. $Cl^-(H_2O) + CD_3Cl$	2.58×10^{-13}	5.97
5. $Cl^-(D_2O) + CH_3Cl$	2.53×10^{-13}	6.01
6. $Cl^-(H_2O)_2 + CH_3Cl$	2.48×10^{-12}	10.7
7. $Cl^-(H_2O)_2 + CD_3Cl$	2.46×10^{-12}	10.7
8. $Cl^-(D_2O)_2 + CH_3Cl$	3.12×10^{-12}	11.0

[a] Computed by fitting to $k = A \exp(-E_a/RT)$ at 295 and 305 K.

Results

The conventional and variational transition-state-theory rate constants and kinetic isotope effects (k_H/k_D) at 300 K are given in Table I. Since the effect of hydration on the unsubstituted (i.e., perprotio) reactions has been discussed previously,[12] we concentrate our attention on the effect of isotopic substitution. First of all we see that the deviation of variational from conventional transition-state theory and the extent of tunneling are approximately independent of isotopic substitution so we can use any of the three levels of theory; we will use the most reliable level, CVT/SCSAG.

Reactions 2, 4, and 7 show the effect of α-deuterium substitution at the reaction center. The isotope effect is inverse ($k_H/k_D < 1$). Interestingly, the deviation of k_H/k_D from unity is almost twice as large with two waters present ($n = 2$) as for the bare solute ($n = 0$); this trend as well as the reason for the inverse effect will be analyzed below.

Reactions 5 and 8 show the effect of using heavy water. The KIE is particularly large for $n = 2$.

Table II shows that most of the KIEs are only weakly dependent on temperature, with the heavy-water effect for $n = 2$ providing a striking exception. Table III presents Arrhenius activation parameters for all reactions, and it shows that addition of a second heavy water has significant effect on both Arrhenius parameters.

(18) Wigner, E. *J. Chem. Phys.* **1937**, *5*, 720. Keck, J. C. *Adv. Chem. Phys.* **1967**, *13*, 85. Truhlar, D. G.; Garrett, B. C. *Acc. Chem. Res.* **1980**, *13*, 440.

(19) Garrett, B. C.; Truhlar, D. G. *J. Chem. Phys.* **1979**, *70*, 1593; *J. Phys. Chem.* **1979**, *83*, 1079.

(20) Garrett, B. C.; Truhlar, D. G.; Grev, R. S.; Magnuson, A. W. *J. Phys. Chem.* **1980**, *84*, 1730.

(21) Truhlar, D. G.; Isaacson, A. D.; Garrett, B. C. In *Theory of Chemical Reaction Dynamics*; Baer, M., Ed.; CRC Press: Boca Raton, FL, 1985; Vol. IV, p 65.

(22) Kreevoy, M. M.; Truhlar, D. G. In *Investigation of Rates and Mechanisms of Reactions*, 4th ed., Part I; Bernasconi, C. F., Ed.; Wiley: New York, 1986; p 13. Tucker, S. C.; Truhlar, D. G. In *New Theoretical Concepts for Understanding Organic Reactions*; Bertrán, J., Csizmadia, I. G., Eds.; Kluwer: Dordrecht, 1989; p 291.

(23) Eyring, H. *J. Chem. Phys.* **1935**, *3*, 107.

(24) Isaacson, A. D.; Truhlar, D. G.; Rai, S. N.; Steckler, R.; Hancock, G. C.; Garrett, B. C.; Redmon, M. *J. Comput. Phys. Commun.* **1987**, *47*, 91. Isaacson, A. D.; Truhlar, D. G.; Rai, S. N.; Hancock, G. C.; Lauderdale, J. G.; Truong, T. N.; Joseph, T.; Garrett, B. C.; Steckler, R. *Research Report UMSI 88/87*, University of Minnesota Supercomputer Institute, Minneapolis, 1988.

(25) Skodje, R. T.; Truhlar, D. G.; Garrett, B. C. *J. Phys. Chem.* **1982**, *86*, 1136. Truhlar, D. G.; Isaacson, A. D.; Skodje, R. T.; Garrett, B. C. *J. Phys. Chem.* **1982**, *86*, 2252.

Table IV. Factor Analysis of the KIEs at 300 K

reaction	KIE	k_H/k_D	factors				
			η_κ	η_{trans}	η_{rot}	η_{vib}	η_{pot}
2. $Cl^- + CD_3Cl$	k_1/k_2	0.95	0.989	1.04	1.22	0.76	1.00
4. $Cl^-(H_2O) + CD_3Cl$	k_3/k_4	0.94	0.994	1.05	1.69	0.53	1.00
5. $Cl^-(D_2O) + CH_3Cl$	k_3/k_5	1.04	1.00	1.03	1.41	0.72	1.00
7. $Cl^-(H_2O)_2 + CD_3Cl$	k_6/k_7	0.91	0.985	1.05	1.71	0.51	1.00
8. $Cl^-(D_2O)_2 + CH_3Cl$	k_6/k_8	1.24	0.985	1.03	1.03	1.19	1.00

Analysis

In order to understand these results we carried out factor analyses[26,27] of the KIEs. In particular we note that[21,22]

$$k^{CVT/SCSAG} = \kappa^{SC}\frac{\sigma\tilde{k}T}{h}R_{trans}R_{rot}R_{vib}\exp(-V^{CVT}/N_A\tilde{k}T) \quad (2)$$

where σ is a symmetry factor, $\tilde{k}$ is Boltzmann's constant, T is temperature, h is Planck's constant, R_{trans} is the ratio of the translational partition function for the variational transition state to that for reactants, R_{rot} and R_{vib} are similar ratios for rotational and vibrational degrees of freedom, V^{CVT} is the molar potential energy at the variational transition state, and N_A is Avogadro's number. Noting that σ is independent of isotopic substitution for the cases considered in this article, the ratio of the rate constant for the undeuterated reaction to that for the deuterated one may be written as

$$k_H/k_D = \eta_\kappa\eta_{trans}\eta_{rot}\eta_{vib}\eta_{pot} \quad (3)$$

where

$$\eta_\kappa = \kappa_H^{SC}/\kappa_D^{SC} \quad (4)$$

$$\eta_X = R_{X,H}/R_{X,D}\ (X = \text{trans, rot, or vib}) \quad (5)$$

and

$$\eta_{pot} = \exp[-(V_H^{CVT} - V_D^{CVT})/N_A\tilde{k}T] \quad (6)$$

The results of the factor analysis at 300 K are shown in Table IV. This table shows clearly that the KIEs are usually dominated by vibrational effects, usually partly cancelled by an opposing rotational effect. The only exception to vibrational dominance occurs for the solvent KIE with one water (k_3/k_5), where rotational effects dominate. (However, the expression of KIE factors as percentages can be misleading since the normal rotational KIE effect of 41% is almost completely cancelled by the inverse vibrational effect of 28%.) The only case where rotational and vibrational effects do not partly cancel is k_6/k_8, where—unlike the other KIEs—the ratio η_{vib} is normal. Since the qualitative explanations of KIEs are usually based on vibrational effects, the factor analysis of Table IV provides a very important example of how such explanations can be misleading. Thus the vibrational effects are much larger for k_3/k_4 and k_6/k_7, about a factor of 2, than for k_6/k_8, about 20%, even though the net KIE is less than 10% for k_3/k_4 and k_6/k_7 but is 24% for k_6/k_8.

In order to achieve a more detailed understanding we further factor η_{vib} into contributions from individual vibrational modes. For reactant modes we write

$$\eta^R_{vib,m} = Q^R_{vib,m,D}/Q^R_{vib,m,H} \quad (7)$$

for each mode m, where $Q^R_{vib,m}$ is the vibrational partition function for mode m of reactants with zero of energy at the classical equilibrium geometry of reactants. For transition-state modes we write

$$\eta^{CVT}_{vib,m} = \frac{Q^{GT}_{vib,m,H}(s^{CVT}_{*,H})}{Q^{GT}_{vib,m,D}(s^{CVT}_{*,D})} \quad (8)$$

Table V. Harmonic Reactant Vibrational Frequencies (cm^{-1}) for Reaction with One Water

mode	$Cl^-(H_2O)$	$Cl^-(D_2O)$	CH_3Cl	CD_3Cl
1	3919	2860	3092	2295
2	3681	2673	3092	2295
3	1758	1281	2981	2134
4	603	438	1453	1051
5	269	194	1453	1051
6	132	126	1377	1044
7			1017	765
8			1017	765
9			741	703

Table VI. Harmonic Saddle Point Vibrational Frequencies (cm^{-1}) for Reaction with One Water

mode	$ClCH_3Cl(H_2O)^-$	$ClCD_3Cl(H_2O)^-$	$ClCH_3Cl(D_2O)^-$
1	3854	3854	3309
2	3751	3751	3307
3	3309	2472	3105
4	3307	2470	2823
5	3105	2196	2716
6	1701	1670	1394
7	1388	1023	1384
8	1384	1019	1234
9	1023	737	1023
10	950	674	950
11	948	672	948
12	422	450	312
13	363	363	259
14	328	328	232
15	231	228	231
16	211	197	211
17	206	189	206
18	113	91	112
19	92	83	88
20	47	47	46
21	584i	583i	584i

Table VII. Harmonic Reactant Vibrational Frequencies (cm^{-1}) for Reaction with Two Waters

mode	$Cl^-(H_2O)_2$	$Cl^-(D_2O)_2$	mode	$Cl^-(H_2O)_2$	$Cl^-(D_2O)_2$
1	3875	2828	9	486	350
2	3776	2759	10	457	329
3	3646	2647	11	266	196
4	3586	2607	12	254	185
5	1814	1321	13	179	165
6	1717	1251	14	135	130
7	787	567	15	80	78
8	728	532			

where $Q^{GT}_{vib,m}(s)$ is the vibrational partition function for mode m of the generalized transition state at a distance s along the reaction path with zero of energy at the minimum potential for that transition state, and $s = s_*^{CVT}$ is the variational location of the transition state. Then

$$\eta_{vib} = \prod_{m=1}^{3N-M}\eta^R_{vib,m}\prod_{m=1}^{3N-7}\eta^{CVT}_{vib,m} \quad (9)$$

where N is the total number of atoms and M is the number of translations and rotations of reactants (M equals 9 for $n = 0$ and 12 for $n = 1$ or 2).

Tables V–IX give the vibrational frequencies for all reactants and saddle point modes. Table X gives the factors of eqs 7–9.

(26) Garrett, B. C.; Truhlar, D. G.; Magnuson, A. W. *J. Chem. Phys.* **1982**, *76*, 2321. Tucker, S. C.; Truhlar, D. G.; Garrett, B. C.; Isaacson, A. D. *J. Chem. Phys.* **1985**, *82*, 4102.

(27) Lu, D.-h.; Maurice, D.; Truhlar, D. G. *J. Am. Chem. Soc.* **1990**, *112*, 6206.

Table VIII. Harmonic Saddle Point Vibrational Frequencies (cm^{-1}) for Reaction with Two Waters

mode	$ClCH_3Cl(H_2O)_2^-$	$ClCD_3Cl(H_2O)_2^-$	$ClCH_3Cl(D_2O)_2^-$
1	3860	3860	3308
2	3856	3856	3307
3	3755	3755	3104
4	3754	3754	2828
5	3308	2471	2825
6	3307	2470	2719
7	3104	2196	2718
8	1699	1698	1399
9	1689	1687	1392
10	1391	1024	1234
11	1389	1022	1223
12	1025	739	1024
13	952	676	952
14	950	674	950
15	413	413	302
16	395	387	300
17	361	361	257
18	357	356	254
19	324	325	235
20	315	315	230
21	235	234	223
22	219	201	219
23	204	190	204
24	153	112	148
25	90	90	87
26	86	86	82
27	44	44	43
28	43	43	42
29	22	22	22
30	669i	668i	669i

Table IX. Harmonic Saddle Point Frequencies for Reaction without Water

mode	$ClCH_3Cl^-$	$ClCD_3Cl^-$	mode	$ClCH_3Cl^-$	$ClCD_3Cl^-$
1	3309	2472	7	947	671
2	3309	2472	8	947	671
3	3106	2197	9	220	220
4	1381	1018	10	206	190
5	1381	1017	11	206	190
6	1021	735	12	469i	469i

The rows are labeled by reactant or saddle point frequencies (cm^{-1}) of the perprotio case with $n = 2$, i.e., reaction 6 in the convention used in the tables.

Since several of the modes with frequencies below 500 cm^{-1} cross and may interact strongly as the system progresses along the reaction path, their effects are multiplied together, i.e.

$$\eta_{vib,low} = \left(\prod_{m=M^R+1}^{3N-M} \eta^R_{vib,m}\right)\left(\prod_{m=M^{GT}+1}^{3N-M} \eta^{CVT}_{vib,m}\right)\left(\prod_{m=3N-M+1}^{3N-7} \eta^{CVT}_{vib,m}\right) \quad (10)$$

where N and M are as in eq 9, N^R is the number of atoms in the molecular reactant, M^R or M^{GT} is the number of modes of reactant or generalized transition state respectively with frequency above 500 cm^{-1}, the first two factors in (10) represent the overall contribution of low-frequency modes present in both the reactants and the generalized transition state, and the third factor is the overall contribution of transitory modes which do not correlate with bound vibrational modes or reactants. We also define the contribution of high-frequency modes as

$$\eta_{vib,high} = \left(\prod_{m=1}^{M'} \eta^R_{vib,m}\eta^{CVT}_{vib,m}\right) \quad (11)$$

where M' is the number of modes with frequencies above 2000 cm^{-1}. Finally the contribution of mid-frequency modes is defined by

$$\eta_{vib,mid} = \eta_{vib}/(\eta_{vib,low}\eta_{vib,high}) \quad (12)$$

This separation into three ranges of modes is well-defined because there are no modes of reactants or saddle point for any of the reactions 1–8 with frequencies in the range 487–531 cm^{-1} or in the range 1815–2133 cm^{-1}, only one mode moves from one of the three groups to another upon isotopic substitution (this mode, the 603-cm^{-1} mode of $Cl^-(H_2O)$, which decreases to 438 cm^{-1} upon isotopic substitution, is treated as a mid-frequency mode in the present analysis), and no modes move in or out of the high-frequency group as the system proceeds from reactants to the transition state. (Although the number of modes in the low- and mid-frequency ranges is not conserved, no modes which retain a recognizable character move from one group to another.) The high-frequency modes are C–H and O–H stretches, and the mid-frequency modes are CH_3 modes, the C–Cl stretch, and, for $n \neq 0$, water bends and some of the water librations. The three factors and their products are compared in Table XI.

Although, of course, the higher frequency modes give larger effects when we look at reactants and transition states separately, as in Table X, this would not necessarily imply that these modes make the largest contributions to the KIE since there is considerable cancellation of these contributions. Table XI shows in fact that for k_1/k_2 the net effect of high-frequency modes nearly cancels for one of the solvent KIEs, is 19% for the other, and is 29% for the unhydrated and microhydrated CH_3/CD_3 effects.

Table X. Factorization of η_{vib} at 300 K[a]

mode	k_1/k_2	k_3/k_4	k_3/k_5	k_6/k_7	k_6/k_8
		CH_3Cl Modes ($\eta^R_{vib,m}$)			
3092	6.75	6.75	1.00	6.75	1.00
3092	6.75	6.75	1.00	6.75	1.00
2981	7.61	7.61	1.00	7.61	1.00
1453	2.64	2.64	1.00	2.64	1.00
1453	2.64	2.64	1.00	2.64	1.00
1377	2.23	2.23	1.00	2.23	1.00
1017	1.86	1.86	1.00	1.86	1.00
1017	1.86	1.86	1.00	1.86	1.00
741	1.10	1.10	1.00	1.10	1.00
		$Cl^-(H_2O)_n$ Modes ($\eta^R_{vib,m}$)			
3875		1.00	12.7	1.00	12.4
3776				1.00	11.5
3646		1.00	11.2	1.00	11.0
3586				1.00	10.5
1814				1.00	3.26
1717		1.00	3.14	1.00	3.06
787				1.00	1.77
728		1.00	1.60	1.00	1.68
under 500		1.00[b]	1.50[b]	1.00[c]	5.41[c]
		Generalized Transition State Modes ($\eta^{CVT}_{vib,m}$)			
3860				1.00	0.0838
3856		1.00	0.0842	1.00	0.0846
3755				1.00	0.0837
3754		1.00	0.0838	1.00	0.0831
3308	0.135	0.135	1.00	0.134	1.00
3307	0.135	0.135	1.00	0.135	1.00
3104	0.113	0.113	1.00	0.113	1.00
1699		0.994	0.325	0.994	0.327
1689				0.994	0.326
1391	0.416	0.415	1.01	0.413	1.02
1389	0.416	0.415	1.00	0.413	1.01
1025	0.492	0.492	1.00	0.492	0.999
952	0.500	0.502	1.00	0.500	1.00
950	0.500	0.500	1.00	0.502	1.00
under 500	0.846[d]	0.596[e]	0.290[e]	0.589[f]	0.0830[f]

[a] Calculated from eq 7 for reactant modes and eq 8 for the modes of the generalized transition state. [b] Two modes. [c] Seven modes. [d] Three modes. [e] Nine modes. [f] Fifteen modes.

Table XI. Factorization of η_{vib} at 300 K for Correlated and Transitory Modes

reaction	KIE	η_{vib}	factors		
			$\eta_{vib,low}$	$\eta_{vib,mid}$	$\eta_{vib,high}$
2. $Cl^- + CD_3Cl$	k_1/k_2	0.76	0.85	1.26	0.71
4. $Cl^-(H_2O) + CD_3Cl$	k_3/k_4	0.53	0.60	1.25	0.71
5. $Cl^-(D_2O) + CH_3Cl$	k_3/k_5	0.72	0.43	1.65	1.00
7. $Cl^-(H_2O)_2 + CD_3Cl$	k_6/k_7	0.51	0.59	1.23	0.71
8. $Cl^-(D_2O)_2 + CH_3Cl$	k_6/k_8	1.19	0.45	3.25	0.81

For the unhydrated CH_3/CD_3 kinetic isotope effect, Tables IV and XI show that the 29% effect of the high-frequency modes is the single factor most responsible for the inverse KIE. This effect receives additional support from a 15% inverse contribution due to low-frequency modes, and it is opposed primarily by a 22% normal effect due to rotations and a 26% normal effect due to mid-frequency modes. The other modes (translation and the reaction coordinate) make a cumulative contribution of only 2%.

Next consider the effect of adding a single solvent molecule on the secondary KIE corresponding to substitution of CH_3 by CD_3. The rough constancy of this KIE, 0.94 for $n = 1$ vs 0.95 for $n = 0$, is due to a significant decrease in the vibrational contribution; otherwise the increasing rotational contribution (see Table IV, 1.69 vs 1.22) would change the KIE to normal. The overall vibrational factor for k_3/k_4 is 0.53 as compared to 0.76 for k_1/k_2. Clearly, from Tables X and XI, this change results mainly from a change in the low-frequency modes of the transition states. In fact the effect of microhydration on the secondary KIE is traceable almost entirely to a single transition-state mode, the twist of CH_3 or CD_3 around the Cl–Cl axis. The twist mode is a rotation in the absence of solvent, but the presence of water converts it into a low-frequency vibration. This mode also dominates the change of the KIE from k_1/k_2 to k_6/k_7 when one more solvent molecule is added. This mode has frequencies of 113, 91, 152, and 112 cm^{-1} for reactions 3, 4, 6, and 7, respectively.

Now consider the solvent KIEs. Reactions 5 and 8 involve deuterium substitution in the solvent. The overall vibrational contributions for these reactions are not simple—for k_3/k_5, η_{vib} is inverse, but for k_6/k_8, it is normal. The change of the vibrational contribution from inverse to normal by adding one more solvent molecule is due to mid-frequency modes; their contribution varies from 1.65 for k_3/k_5 to 3.25 for k_6/k_8 (see Table XI). In this case the effect can be traced almost entirely to two modes, both water librational modes of the solvated Cl^- reactant. One, at 787 cm^{-1}, corresponds to an out-of-plane bend of the water–water hydrogen bond[28] (see Figure 1), and the other, at 728 cm^{-1}, corresponds to the water–Cl^- bending motion. This is a good example of an initial-state effect since both modes correlate adiabatically with very different lower frequency transition-state modes that are less isotopically sensitive.

One important question answered by the above analysis is whether the solvent KIE is rotational, direct vibrational, or indirect vibrational. An indirect vibrational effect would be associated with isotopic substitution in the solvent changing the solute vibrational frequencies by mode mixing. A direct effect is associated with modes in which the solvent participates directly, e.g., stretching of the $Cl^-\cdots HOH$ solvation coordinate. The above discussion and Table IV show that the normal solvent KIE for $n = 1$ is attributable to a rotational effect, and the increase for $n = 2$ is primarily an initial-state direct vibrational effect.

Discussion

α-Deuterium Substitution. The conventional interpretation of α-deuterium secondary KIEs focuses on the hybridization at the α-carbon.[29-38] When this is changing from sp^3 to sp^2, as in S_N2 reactions, one would "ordinarily" expect a normal KIE for $N^- + CH_3X$ due to a decrease in H–C–H and H–C–X bending force constants in proceeding from reactant to transition state, although there is some counterbalancing by increasing N–C–H bending force constants. Most quantitative discussions of α-deuterium secondary KIES on S_N2 or S_N1 reactions have focussed on leaving group participation in and influence on CH_3 deformation modes affected by such force constants. In fact α-deuterium KIEs on bimolecular substitution reactions at methyl are typically inverse,[38-40] with values reported as low as 0.87,[30] but are sometimes normal, with values as large as 1.10 reported.[32] (The "experimental" value for the present reaction is inferred by a Marcus theory analysis to be 0.97.[39]) The inverse effects have been interpreted as indicating that "the bending motion of the α-hydrogen may be more constrained in an S_N2 transition state than in the reactant",[36] but it has also been stated that, even when the KIE is inverse, "the information given by k_H/k_D is clear" and "a larger k_H/k_D indicates a transition state in which the out-of-plane bend of the α-hydrogen is less encumbered than in the reactant".[38] The Arrhenius parameters of the KIE are also sensitive to the C–H stretching force constant.[33]

The analysis presented in the previous section provides an ab initio test of the conventional model for k_H/k_D values and whether these result primarily from the out-of-plane bend (i.e., the umbrella mode of the transition state), the H–C–H bends, or the C–H stretch. The CH_3 deformations (including the H–C–H bends and the umbrella mode) are modes 4–8 at the $n = 0$ transition state, 7–11 at the $n = 1$ transition state, 10–14 at the $n = 2$ transition state, and 4–8 in CH_3Cl. Multiplying the mode-specific KIEs (i.e., the $\eta_{vib,m}^{CVT}$ and $\eta_{vib,R}^{R}$ factors of Table X) for these modes yields 1.14 for k_1/k_2 and k_3/k_4 and 1.13 for k_6/k_7. Thus these modes actually contribute to a normal KIE, which follows from the fact that they all decrease in frequency. The C–H stretches are modes 1–3 for the transition states with $n = 0$, 3–5 for $n = 1$, 5–7 for $n = 2$, and 1–3 for CH_3Cl. Multiplying the six corresponding mode-specific KIEs yields 0.71 for all three reactions (see Table XI). As a result the C–H stretches are the dominant contributor to the inverse α-deuterium KIEs for the unhydrated S_N2 reaction, and they contribute almost as much as the cumulative effect of all low-frequency modes for the microhydrated cases (again see Table XI). In all three cases, if we simply omitted the contribution of the C–H stretches, the net KIE would be normal rather than inverse. Inverse KIEs result from isotopically sensitive vibrational modes that increase in frequency, in proceeding from reactants to the variational transition state, which the C–H stretches do in the ab initio calculations on which our potential energy function is based. In particular the scaled ab initio frequencies for the C–H stretches increase by 125–217 cm^{-1} in proceeding from the reactants to the transition state.[14] This increase is consistent with the transition state H—$C(sp^2)$ bonds being stronger than the reactant H—$C(sp^3)$ bonds, and it implies that C—H bonds in $R_2C{=}CRH$ systems are a better model than those in O=CRH systems for the C—H bonds at the present transition state.

The only other α-deuterium KIEs studied by variational transition-state theory are the reactions $CH_4/CD_3H + H/D \rightarrow CH_3/CD_3 + H_2/HD$.[27] In these cases, in addition to large tunneling effects, there was a very significant difference in the overbarrier KIE between the variational and conventional transition-state calculations. In the present case, in contrast, the variational and tunneling effects on the KIE are negligible. Nevertheless there are also similarities between these two cases. The C–H stretches, for example, contribute an inverse factor of 0.70 at the level of conventional transition-state theory, although they contribute a normal factor of 1.18 to k_H/k_D in the canonical variational calculation for the $CH_4/CD_3H + H \rightarrow H_2 + CH_3/CD_3$ case. As a result the best estimate of the non-tunneling α-deuterium secondary KIE is 1.22, so again the stretches are very important in determining the overall effect.

(28) This mode also occurs in the isolated water dimer as analyzed by: Reimers, J. R.; Watts, R. O. *Chem. Phys.* **1984**, *85*, 83. In the notation of that reference it is ν_{10}.
(29) Streitweiser, A., Jr.; Jagow, R. H.; Fahey, R. C.; Suzuki, S. *J. Am. Chem. Soc.* **1958**, *80*, 2326.
(30) Llewellyn, J. A.; Robertson, R. E.; Scott, J. W. M. *Can. J. Chem.* **1960**, *38*, 222.
(31) Weston, R. E., Jr. *Annu. Rev. Nucl. Sci.* **1961**, *11*, 439.
(32) Seltzer, S.; Zavitsas, A. A. *Can. J. Chem.* **1967**, *45*, 2023.
(33) Willi, A. V.; Won, C. M. *J. Am. Chem. Soc.* **1968**, *90*, 5999.
(34) Scheppele, S. E. *Chem. Rev.* **1972**, *72*, 511.
(35) Buddenbaum, W. E.; Shiner, V. J., Jr. In *Isotope Effects on Enzyme Catalyzed Reactions*; Cleland, W. W., O'Leary, M. H., Northrup, D. B., Eds.; University Park Press: Baltimore, 1977; p 1.
(36) Melander, L.; Saunders, W. H. *Reaction Rates of Isotopic Molecules*; Wiley: New York, 1980.
(37) Yamataka, H.; Tamura, S.; Hanafusa, T.; Ando, T. *J. Am. Chem. Soc.* **1985**, *107*, 5429.
(38) Saunders, W. H., Jr. In *Investigation of Rates and Mechanisms of Reactions*, 4th ed., Part I; Bernasconi, C. F., Ed.; Wiley: New York, 1986; p 565.
(39) Albery, W. J.; Kreevoy, M. M. *Adv. Phys. Org. Chem.* **1978**, *16*, 87.
(40) Thornton, E. R. *Annu. Rev. Phys. Chem.* **1966**, *17*, 349.

Solvent KIEs. Aqueous solvent KIEs have been extensively analyzed for reactions involving exchangeable protons, and they reflect the fractionation of D into the solute and transition state relative to water. Solvent KIEs that reflect nonreactive solvation effects have also been studied, but they are harder to analyze.[31,40-43] The microsolvent KIEs on reactions 3 and 6 are of the latter type. Since our solvent–solute coupling potential is not as reliable as our solute force field, our results for the microsolvent KIEs are correspondingly more uncertain as well. Nevertheless we believe that this kind of calculation leads to interesting insight into the factors which must be considered in interpreting microsolvent KIES, and we hope they provide a stimulus for measuring these effects as a way to test force fields that might also be used to study bulk solvent KIEs. In addition it would be interesting to test the sensitivity of the present result for the cluster microsolvent KIE with $n = 2$ to improvements in the potential energy functions for the water interactions.

One possible source of solvent KIEs in S_N2 reactions is solvent reorganization at sites of changing charge character.[39-41,44] Another, partly equivalent, possibility is the change in frequencies of librational degrees of freedom of the water molecules as reaction progresses.[45]

On the basis of earlier work by Swain and Bader,[45] Schowen[42] has proposed a simple method for solvent KIEs of hydrolysis reactions. These workers modeled the solvent KIE in terms of the effect of ionic charges on water librations, assuming, in good accord with more recent studies,[46] that the water-structure-breaking effect of a solute is dominated by the first hydration shell, in which water is held more loosely than in the absence of solute. In this model, since we are proceeding to a transition state in which charge is more dispersed than in reactants, the water structure will be strengthened in the transition state, and the kinetic isotope effect will be inverse. Schowen assumes that each inner-sphere water of hydration contributes a factor of $(1.5)^{(|q^*|-|q^R|)/4}$ to k_H/k_D, where q^* is the charge solvated in the transition state, and q^R is the charge solvated in the reactants. In the cases considered here, $|q^R|$ is unity, but $|q^*|$ is unclear since the water is bridging the whole delocalized charge distribution consisting of two chlorides, each with $q = -0.7$, and the methyl group, with $q = +0.4$. If the perturbation of water structure by the charge-delocalized transition state were less than that by the localized charge in reactants, one would calculate by this model that $(1.5)^{-2/4} \leq k_H/k_D \lesssim 1$ for $n = 2$, which yields 0.82–1.00. This can be compared to the present results for the product $\eta_{vib,low}\eta_{vib,mid}$, which equals 1.46 for k_6/k_8. Clearly, as seen in Table X and discussed above, many modes contribute to the solvent KIE in the present case, and this bulk water model is not applicable to the microhydrated reactions studied here. In fact, even though charge is dispersed in proceeding to the transition state, we find normal rather than inverse solvent KIEs for the present potential energy function and dynamics treatment. This is consistent with the fact that for the microhydrated reactant with $n = 2$, there is actually more water structure breaking at the transition state, where the water dimer hydrogen bond is broken, than for the reactant, where it is not.

In liquid water the differences in water–water modes between the reactant and the transition state may be quite different than observed here where a water–water hydrogen bond is fully broken in proceeding to the transition state. In both microhydrated reactions and bulk water the solvent kinetic isotope effect may give unique information about such water-structure breaking at reactants and transition states.

Concluding Remarks

We have seen that the origins of kinetic isotope effects for microhydrated reactions can be understood in intimate detail. Rotations and identifiable vibrational modes are found to be very important. The inverse α-deuterium KIE for the unhydrated S_N2 reactions at methyl is attributable to C–H stretches, whose role is neglected in most previous models, and not to tightening of the CH_3 deformations. The C–H stretches also make a critical contribution to the inverse α-deuterium KIE for the microhydrated S_N2 reactions with one or two water molecules, and one would assume that this C–H stretch effect is also very important for reactions in solution. The solvent KIE is attributable to the CH_3 internal rotation around the Cl–Cl axis for the case of solvation by one water and to H_2O librations in the initial state for the case of two waters. In bulk solution the solvent KIEs may be dominated by other motions since in bulk solution the solvent molecules are not expected to carry out the large-scale migrations observed in the microhydrated gas-phase reactions. Nevertheless it is quite interesting that the widely discussed phenomenon of solvent structure breaking plays an important role at the transition state of the microhydrated reaction with the absolute minimum number, two, of solvent molecules required for it to be possible. Experimental measurements of the solvent KIEs for microhydrated reactions would provide a very challenging test for solvation force fields.

Acknowledgment. The authors are grateful to M. M. Kreevoy and Angels Gonzalez-Lafont for discussions of many relevant issues. This work was supported in part by the U.S. Department of Energy, Office of Basic Energy Sciences and a graduate fellowship to X. G. Zhao supported by Air Products Foundation.

(41) Laughton, P. M.; Robertson, R. E. In *Solvent Isotope Effects for Equilibria and Reactions*; Coetzee, J. F., Ritchie, C. D., Eds.; Marcel Dekker: New York, 1969; p 399.
(42) Schowen, R. L. *Prog. Phys. Org. Chem.* **1972**, *9*, 275.
(43) Blandamer, M. J.; Burgess, M.; Clare, N. P.; Duce, P. P.; Gray, R. P.; Robertson, R. E.; Scott, J. W. M. *J. Chem. Soc., Faraday Trans. 1* **1982**, *78*, 1103. Blandamer, M. J.; Burgess, J.; Robertson, R. E.; Koshy, K. M.; Ko, E. C. F.; Golinkin, H. S.; Scott, J. M. W. *J. Chem. Soc., Faraday Trans. 1* **1984**, *80*, 2287.
(44) Swain, C. G.; Thornton, E. R. *J. Am. Chem. Soc.* **1962**, *84*, 822.
(45) Swain, C. G.; Bader, R. F. W. *Tetrahedron* **1960**, *10*, 182, 200.
(46) Collins, K. D.; Washabaugh, M. W. *Q. Rev. Biophys.* **1985**, *18*, 323.